Ocean and Coastal Research

ORIGINAL ARTICLE

https://doi.org/10.1590/2675-2824069.20-338mss
ISSN 2675-2824

Active mechanisms controlling morphodynamics of a coastal barrier: Ilha Comprida, Brazil

Mayara Santana Silva[1,*], Carlos Conforti Ferreira Guedes[1], Gyrlene Aparecida Mendes da Silva[2], Gilberto Pessanha Ribeiro[2]

[1] Universidade Federal do Paraná, Departamento de Geologia, Setor de Ciências da Terra (R. Evaristo F. Ferreira da Costa - Jardim das Américas - 81530-001 - Curitiba -PR - Brazil)
[2] Universidade Federal de São Paulo, Departamento de Ciências do Mar (Rua Carvalho de Mendonça, 144 - Vila Belmiro - Santos - SP - Brazil)

*Corresponding author: mayara.santana@ymail.com

ABSTRACT

The Cananéia-Iguape lagoon-estuarine system, where the Ilha Comprida barrier (IC) is located, is one of the most dynamic coastal areas on the southeastern Brazilian coast. IC island is a 63 km-long barrier and it is limited by the Icapara inlet to the north, and the Cananéia inlet to the south. This system has been affected by intense changes in its morphology since the opening of the Valo Grande artificial channel in 1852 A.D., connecting the nearby Ribeira de Iguape river to the Mar Pequeno lagoon. In this context of anthropogenic disturbance on the coastal systems, the objective of this study is to understand the active mechanisms, both natural and anthropogenic, controlling the morphological changes of the northeastern portion of the IC, from monthly as well as centenary timescales. We analyzed successional addition and erosion of beach ridges using a multi-temporal dataset obtained by Optically Stimulated Luminescence, aerial photos (1962 and 2000), satellite images (1980–2016) and GNSS surveys (2015–2017). The results were compared to climatic (rainfall and waves) data. Northeastward migration rates of the IC ranged from 15.5 m/y, on the GNSS surveys, to 154 m/y, calculated based on OSL rates. Changes on rates on the northeastward inlet migration barrier are related to anthropogenic interference, mainly the Valo Grande opening and climate changes. Sediment accumulation occurred mainly during the summer on the baymouth spits. This depositional scheme is consistent with the highest values of Ribeira de Iguape river flow and the low synergy of waves coming from the South. By contrast, the retrogradation of the coastline occurs in the winter, when the wave power is stronger than in the summer. This seasonal configuration is controlled both by the bidirectional longshore drift and by the fluvial discharge.

Descriptors: Optically Stimulated Luminescence, beach ridges, El Niño, anthropogenic influence.

INTRODUCTION

Coastal barriers can be defined as a range of emergent depositional landforms separated from the mainland by a lagoon, bay, or marsh (Davidson-Arnott, 2010). Barriers are also common landforms associated to wave-dominated coasts (Roy et al. 1994). Coastal lagoons and barriers are highly dynamic and vulnerable systems, modulated by the complex interaction between the hydrosphere, lithosphere, atmosphere, and biosphere (Masselink et al., 2014). Natural and anthropogenic forces induce changes in these environments, thus affecting the coastal systems (Dias, 2005; Woodroffe, 2003). Barrier dynamics are directly influenced by the availability of sediments, relative sea level, and processes related to the ocean-atmosphere interaction, such as anomalies related to El Niño/La Niña (Davidson-Arnott, 2010; Masselink et al., 2014).

Submitted on: 11-May-2020
Approved on: 05-January-2021
Associate Editor: Eduardo Siegle

Natural mechanisms acting on coastal dynamic can be measured and analyzed as complex systems (Roy et al., 1994; Woodroffe, 2003) and, in wave-dominated coasts, the wave climate plays a major controlling factor. Herrero et al. (2020) demonstrated that longshore wave power, storminess, and the occurrence of storm groups could be related to progradation rates of beach ridges at Barreta Island (Southern Portugal), where high-energy wave events dominate the temporal control on sediment exchange between beach and inlet deltas. However, Zhang et al. (2014), studying the past 6 ka formation of the Zingst barrier and Darss spit (Northeast Germany), concluded that the evolution of the area is dominated by long-term wind-wave effects rather than short-term storm effects. So, barrier evolution is driven differently regarding regional and local factors (Roy et al., 1994; Woodroffe, 2003), with anthropogenic disturbance growing on recent times and leading to more complex dynamics (Russ and Palinkas, 2020; Zhang et al., 2019).

In this context of anthropogenic disturbance on coastal systems, the Cananéia-Iguape lagoon-estuarine system, on southeastern Brazil, harbors the barrier island of Ilha Comprida (IC). IC island is a 63-km-long barrier, with up to 5 km width, limited by the Icapara inlet, to the north, and the Cananéia inlet, to the south (Geobrás, 1966). (Figure 1). This geomorphic configuration was disrupted in 1852 by the opening of the Valo Grande artificial channel, connecting the Ribeira de Iguape river to the Mar Pequeno lagoon, leading to many environmental (Mahiques et al., 2012) and coastline changes (Geobrás, 1966; Nascimento et al., 2008). A faster northeastward displacement of the Icapara channel, compared with previous conditions, is reported at an approximate rate of 30 m/year, associated with a faster erosion of the Praia do Leste (Geobrás, 1966; Nascimento et al., 2008). However, Ilha Comprida's natural northward (pre-anthropogenic) growing pattern is similar to the current one, as evident from the beach ridge configuration (Guedes et al., 2011a), raising doubts related to the magnitude of anthropogenic influence, as expected with the increased flow at the Icapara inlet. Therefore, the northeastern end of the IC is a great opportunity to study a highly dynamic coast with anthropogenically-influenced changes over time.

The objective of this study is to understand the active mechanisms, both natural, such as climate and wave regime, and anthropogenic interventions on sediment pathways, controlling the morphological changes of the northeast portion of the IC from a seasonal to secular timescale. Also, it aims at determining variations of intensity of these active mechanisms over time, regarding natural and anthropogenic events, and how coastal forces interact on coastal systems. In this paper, a multi-temporal dataset of coastline positions using Global Navigation Satellite System (GNSS) surveys and remote sensing images associated with optically stimulated luminescence (OSL) were compared to atmospheric, oceanographic and hydrological variables. This analysis helped us better understand the active mechanisms controlling the morphodynamics of the northeastern end of the IC over seasonal and secular timescales, with focus on the anthropogenic contribution.

Study area

The regional coastal area, where IC is located, is dominated by wide and long coastal plains and estuaries due to the more inland position of the Serra do Mar (Giannini et al., 2009) with coastal deposits and geomorphology controlled, mainly, by the relative sea-level changes during the Late Quaternary (Muehe, 2012; Suguio and Martin, 1978). The Cananéia-Iguape estuarine system is the largest coastal complex of the São Paulo Bight (Alcantara-Carrio et al., 2017) formed in 5 stages during late Pleistocene and Holocene (Suguio and Martin, 1978). The last stage is associated to the Holocene regressive phase which generated a strandplain (Suguio and Martin, 1994).

Classified as a regressive barrier, the IC shows a northeastward growth pattern registered by a succession of beach ridges (Geobras, 1966; Tessler, 1988; Guedes et al., 2011a). It is composed of Quaternary sandy sediments deposited northeast from a 42-m high hill of Mesozoic intrusive alkaline rocks located at the southwestern end of the barrier (Nascimento et al., 2008; Giannini et al., 2009; Guedes et al., 2011b). Quaternary deposits are composed of a strandplain of fine and very fine sands, as well as sandy-clay fluvio-lagoon deposits and eolian deposits in the southern portion of the island (Suguio and Martin, 1994). The northeastern end of the island is constituted of sand

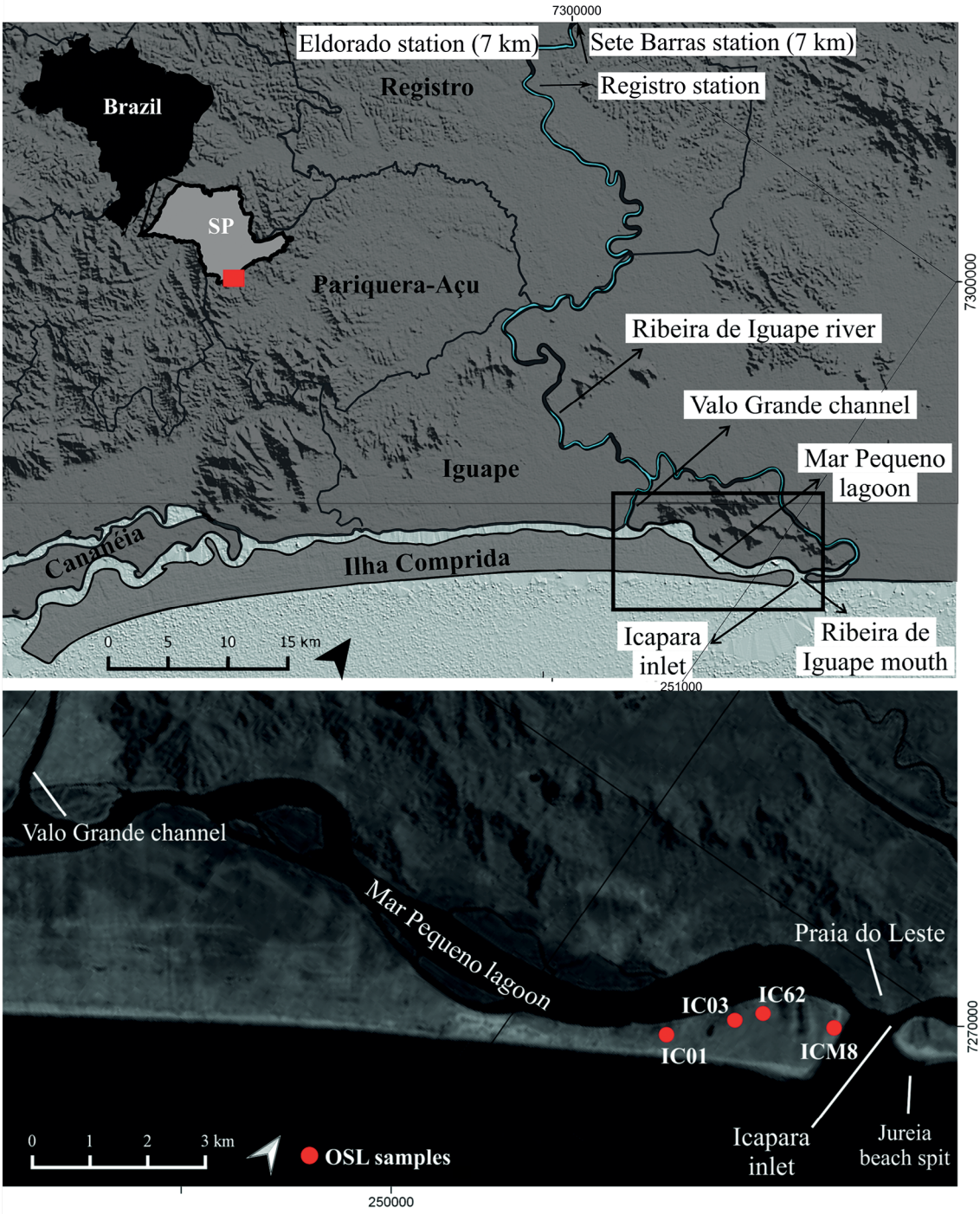

Figure 1. a) Shaded relief of digital elevation model of the Cananéia-Iguape lagoon-estuarine system, with studied area delimitation (black rectangle); b) OSL sampling points represented by the red circles. Source: National Institute of Spatial Research (INPE/Brazil).

partially covered by recent dunes with the presence of vegetation (Geobrás, 1966, Sawakuchi et al., 2008).

The tidal regime of the region comprising the Cananéia-Iguape system is microtidal, with amplitudes ranging from 1.2 meters, on spring tide, to 0.25 meters, on neap (Mesquita and Harari, 1983). The region climate is influenced by atmospheric systems from tropical, subtropical and extratropical genesis.

The rainy season occurs during the area's summer and is influenced by the South American Monsoon System (Vera et al., 2006b; Zhou and Lau, 1998). The rain volume is modulated by the moisture transport from the Atlantic Ocean and the Amazon Basin toward the southeastern region of South America (Marengo et al. 2004). The mean low-level convergence is also reinforced by the transient frontal systems that modulate the South Atlantic Convergence Zone (Carvalho et al., 2004), a diagonal band of maximum precipitation positioned from the northwest to the southeast over the South American continent. Lower precipitation on austral winter, compared with summer, is associated with the weakness of the low-level northwestern monsoon flow, which reduces the moisture transport over subtropical South America. El Niño and La Niña are the major phenomena to play roles and determining the inter-annual climate variability in many regions of South America (Silva and Ambrizzi, 2006; Silva et al., 2009). El Niño/La Niña are also associated to a slight reduction/increase in significant-wave-height (from S and SW) related to the frequency of cold fronts in Rio de Janeiro (Pereira and Klumb-Oliveira, 2015).

The wave climate in the South Atlantic Ocean displays little variability (Hemer et al., 2010). On the Southeastern Brazilian coast, the wave regime is modulated by the passage of frontal systems, mainly by South Atlantic Subtropical High (SASH). In the summer, SASH is better configured and moves slightly to the southwest Atlantic Ocean (Bastos and Ferreira, 2010). During the fall and winter seasons, the passage of cold fronts, associated to a higher frequency of cyclogenesis, intensifies winds, which is reflected in the higher frequency of high wave energy events (Nimer, 1989; Pianca et al., 2010). In the Southeastern sector, waves from the South and the East were dominant in all seasons (Ambrosio et al., 2020; Pianca et al., 2010) with different contributions, due to the synergy of waves (Pianca et al., 2010). This configuration generates a seasonal pattern of longshore transport (Silva et al. 2016). Wave energy gradients affected the evolutionary processes of the inlets, mainly of those related to spit erosion or accretion and to inlet migration (Ambrosio 2020).

The Valo Grande opening, in 1852, aimed at establishing a shortcut between the Iguape harbor and the nearby Ribeira do Iguape river meander, to enable the transport of the regional agricultural and mineral production (Young, 1903). This shortcut shortened the production route by almost 50 km and helped to avoid a stretch of open sea. With initial dimensions of 4 meters wide and 2 meters deep, Valo Grande soon suffered severe erosion and reached 100 m wide and 10 m deep in a few decades (Geobrás, 1966). As a consequence, the Iguape harbor was silted up (Young, 1903) and the Mar Pequeno lagoon suffered environmental changes, such as to salinity and sediment supply (Mahiques et al., 2019. 2012 and 2014). Environmental changes led to changes in fishing and the Ribeira do Iguape river, between Valo Grande and the river mouth, silted up due to decreased flow. As a result, there were two attempts to close it: the first one with the construction of a dam in 1978, which kept the channel closed until 1983; and the second one with spillways in 1990, lasting until 1995 (Schaeffer-Novelli et al., 1990; Simão Jr. et al., 1998). Both structures were disrupted due to flooding events (Simão Jr. et al., 1998).

METHODS

Image analysis

Coastline and barrier area changes, from 1980-2017, were analyzed via Landsat images obtained from Global Visualization Viewer (GloVis) [https://glovis.usgs.gov/] and aerial photos from 1962 (1:25.000 from S.A. Cruzeiro do Sul) and 2000 (1:35.000 from Aerofoto S. A.). Landsat images were selected with a nearly-annual periodicity, depending on the availability of satellite images with low cloud cover (Table 1).

The coastline position, defined as the seaward vegetation line, was measured and determined, manually, using QGIS software. The coastline variation was determined comparatively to a baseline, the 1962 coastline, for five representative sections. Sections I, II and III are located on beaches facing the Icapara inlet and the inflection to open sea; while sections IV and V are located on beaches facing the open sea (Figure 2), perpendicular to the shoreline. The aerial photos and satellite image resolution values were added as the uncertainty values for coastline position.

The barrier area calculation was determined by a coastline polygon on the IC northeastern stretch. Each polygon was limited to the west by a fixed line (Figure 2). Annual area variation rates were estimated

Table 1. Date of the field surveys with GNSS.

Landsat series dates	Sensors	Resolution (meters)
1980 - 1984	Multispectral Scanner System	57
1985 - 1998	Thematic Mapper	30
1999 - 2013	Enhanced Thematic Mapper	15
2013 - 2017	Operational Land Imager/Thermal Infrared Sensor	15

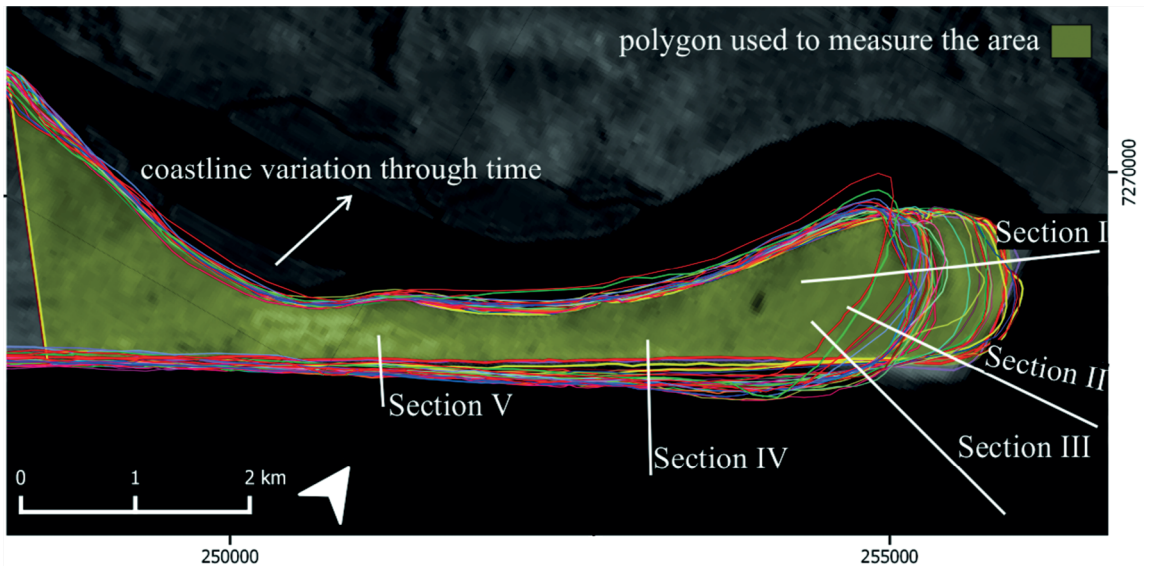

Figure 2. Coastline limits and polygons (colored lines) used in the multi-temporal image analyses for coastline and barrier area.

based on the difference of two polygonal areas divided by the time (years) between the two images.

GNSS SURVEYS

Seven double frequency GNSS surveys were obtained to delimit both the vegetation boundary, defined as the coastline, and changes on the barrier area between surveys, which occurred from May/2015 to March/2017 (Table 2). The Global Navigation Satellite System (GNSS) receptors we used were the GPS Garmin Map 60Cx and GNSS Altus APS-3. Surveys followed orientations from Pinheiro et al. (2008) with a receptor height of 2 meters and storage rate of 1 second. Isolated positioning and cinematic modes were used on the GNSS Altus APS-3 receptor to ensure the geometric accuracy on georeferencing and terrain features recognition (Ribeiro et al., 2004; 2005). All the information obtained in the surveys was processed using the Precise Point Positioning service provided by Geographic and Statistics Brazilian Institute (PPP-IBGE), with expected precision of 0.05 meters for the planimetric coordinates and 0.10 meters for the altimetric component. The data obtained in the field with the GNSS Altus APS-3 receiver were processed based on the proprietary software where geodetic coordinate data (geodesic longitude, latitude and altitude) were generated for each point in the kinematic survey, with a 1s storage interval. The data were arranged in tables with the possibility of importing, reading, interpreting and plotting through the QGIS computational system, generating vector lines in SHP format. They were validated from the less than 3 value by PDOP.

Coastline positions from GNSS surveys were analyzed over six time intervals, between the seven GNSS surveys. From each time interval, accretion and erosion areas were defined by the difference between two surveys polygons and their intersections. Average coastline change was calculated through the sum of the areas (polygons) divided by the coast

Table 2. Date of surveys for each interval and the number of days between each of them.

Surveys	Name	Days between surveys
23/05/2015 to 21/08/2015	Interval I	88
21/08/2015 to 11/11/2015	Interval II	82
11/11/2015 to 13/02/2016	Interval III	94
13/02/2016 to 06/05/2016	Interval IV	83
06/05/2016 to 19/11/2016	Interval V	197
19/11/2016 to 29/03/2017	Interval VI	130

length. Minimum and maximum linear coastline change was measured manually, perpendicular to the shoreline, and informed to show the variability.

Luminescence dating

Luminescence dating was performed on three samples from beach ridges, previously identified by aerial photos, denominated IC62, IC01 and IC03 (Figure 1b). The samplings were made in trenches using aluminum tubes, avoiding the pedogenic horizon and heterogeneities. One superficial sample was collected on the beach (ICM08) for residual OSL signal analysis. All samples were prepared in the Laboratory of Gamma Spectrometry and Luminescence (LEGaL) of the University of São Paulo in Brazil. All laboratorial preparation was performed under red light. Quartz grains were isolated according to the following processes: separation of 120-150 µm sand grains through wet sieving; treatment with H2O2 27%, HCl 3.75%, HF 48-51% for 40 min, to remove organic carbon, CaCO3 and feldspars, respectively; density separation was done with sodium metatungstate to isolate quartz from heavy minerals and feldspars.

The Single Aliquot Regenerative-dose (SAR) protocol (Table 3) (Murray and Wintle, 2000; Wintle and Murray, 2006) was used to determine the equivalent doses on quartz aliquots. Time intervals for quartz OSL decay curves were selected whilst trying to isolate the fast OSL component, applying the early background approach (Cunningham and Wallinga, 2010). The OSL signal was defined as 0 to 0.5 seconds and the background was defined as 0.08 seconds. The choice of time intervals defines the proportion of each component in the net signal, varying in each aliquot due to variations in the intensity and decay rate of each OSL component between grains (Cunningham and Wallinga, 2010).

The dose recovery test was realized to validate OSL dating protocol. A small known dose (45.27 mGy) was applied to simulate the expected small natural dose in four aliquots of sample IC62. Due to the small probable doses, two pre-heat temperatures were tested (180 and 200ºC) to examine the best protocol parameters to charge thermal transfer.

Atmospheric, oceanographic and hydrological dataset

Precipitation data from the Global Precipitation Climatology Centre (GPCC) provided by the NOAA/OAR/ESRL PSD, with a resolution of 0.5°, were used to calculate the accumulated annual and seasonal mean precipitation over Vale do Ribeira (49.3°- 47.2°W; 25.1° - 23.9°S) from 1950 to 2013. El Niño events were selected using the classification of the Climate Prediction Center (CPC)/NOAA, which is based on the Southern Oscillation Index (SOI); events with strong magnitudes were characterized according to Kiladis and Van Loon (1988). El Niño events were analyzed, using the coefficient of determination (R^2), regarding the possible linkages between the annual occurrence of these events when compared to other variables, such as precipitation, river flow and changes to the IC barrier area. Ribeira de Iguape's mean annual river flow, from 1940 to 2016, was obtained from the Departamento de Águas e Energia Elétrica (DAEE) at three different stations: Registro (24° 29′ 27″; 47° 50′ 12″, 35 km from Valo Grande), Eldorado (24° 31′ 00″; 48° 06′ 45″, 57 km from Valo Grande) and Sete Barras (24° 23′ 34″; 47° 55′ 43″, 49 km from Valo Grande).

Offshore wave data was extracted from the global wave generation model WaveWatch III® (WW3®), obtained from the National Oceanic and Atmospheric Administration/National Centers for Environmental Prediction (NOAA/NCEP), ranging from 1979 to 2017.

Table 3. SAR procedure used for equivalent-dose determination.

1. Dose (Di)
2. Pre-heat at 200°C for 10 s
3. LM-OSL at 125°C for 45 s (Ri)
4. Test dose (TDi)
5. Pre-heat at 200°C for 10 s
6. LM-OSL at 125°C for 45s (Ti)
7. Calculate sensitivity-corrected OSL Li=Ri/Ti

To determine the frequency of each wave direction, directional wave histogram data were summarized, on annual and seasonal scales, as significant wave heights and main directions. The wave data also was separated into intervals, from I to VI (Table 2), to correlate the wave regime with accretion and erosion areas calculated by GNSS surveys. The amount of wave power (P, in W/m) was estimated according Salter's (1974) approach. Then, the synergy of wave height (H, in meters) and period (T, in seconds) was used to calculate P in the equation:

$$P = \rho g^2 H^2 T/32\pi \quad (1)$$

where ρ is water density (1.027 kg/m^3), g the acceleration due to gravity (9.8 m/s^2)

RESULTS

GNSS SURVEY RATES

Overall, coastline retrogradation prevails during intervals I, IV and V, while coastline progradation prevails during intervals II and III. Furthermore, the sedimentary balance presents seasonal behavior. The region's nearly inflection between ocean and inlet coasts is marked by alternation between erosion and progradation (Figure 3).

In Interval I (winter), erosion areas were ten times greater than accretion ones, resulting in 17.4x10^3 m^2 of eroded area. On the open sea coastline, an average of 2.5 meters retrogradation occurred. Also, near the inlet, a spot up to 14 meters of progradation and a neighboring zone with up to 15 meters of erosion are observable. Near the Icapara inlet, there is erosion predominance, up to 50 meters, with retrogradation increasing toward the channel (Figure 3a).

Interval II (spring) had a total balance of 774 m^2 of area loss. Even though Interval II presents the smallest gross balance, the intensity of the coastline dynamics was not lower than the other periods. The total eroded area was 13.4x10^3 m^2, slightly higher than progradation (12.7x10^3 m^2) (Figure 3b). With the opposite behavior to Interval I, the ocean shore shows a trend of generalized progradation, with an average of 15 m, and maximum of 45 m. In contrast, the Icapara inlet coast has predominance of retrogradation, with an average of 4 m. Between these distinct areas, at the coastline inflection, there was a marked erosion with up to 80 m of retrogradation.

Progradation was predominant in Interval III (summer, Figure 3c), with a gross area increase of 77x10^3 m^2. Erosion only occurred at the coastline, north of the inflexion, at the Icapara inlet coast. This inflexion, which had been eroded on the last interval, prograded up to 90 m, regaining part of the previously eroded area. On the shore facing the open sea, there was progradation ranging from 40 m in the southwest to 85 m in the northeast.

The period corresponding to interval IV (autumn) was marked by the beginning of an extensive retrogradation phase (Figure 3d). In this interval, no accretion was perceived, with an average retrogradation of 15 m, and maximum of 75 m in the inflection. The sum of the eroded area was 38x10^3 m^2.

This erosive phase proceeds until Interval V (winter and spring, Figure 3e). The total balance was a deficit of 73x10^3 m^2, with just a small progradation spot located in the inflection zone. Both shores, oceanic and facing the channel, presented severe erosion with a mean of 33 m and maximum of 85 m.

The last interval (summer) is represented by a progradational phase (Figure 3f), with a gross accretion of 57x10^3 m^2. Progradation occurs on oceanic beaches with an average of 31 m and maximum of 80 m. In the inflection area, the erosive processes are predominant and up to 18 m of retrogradation

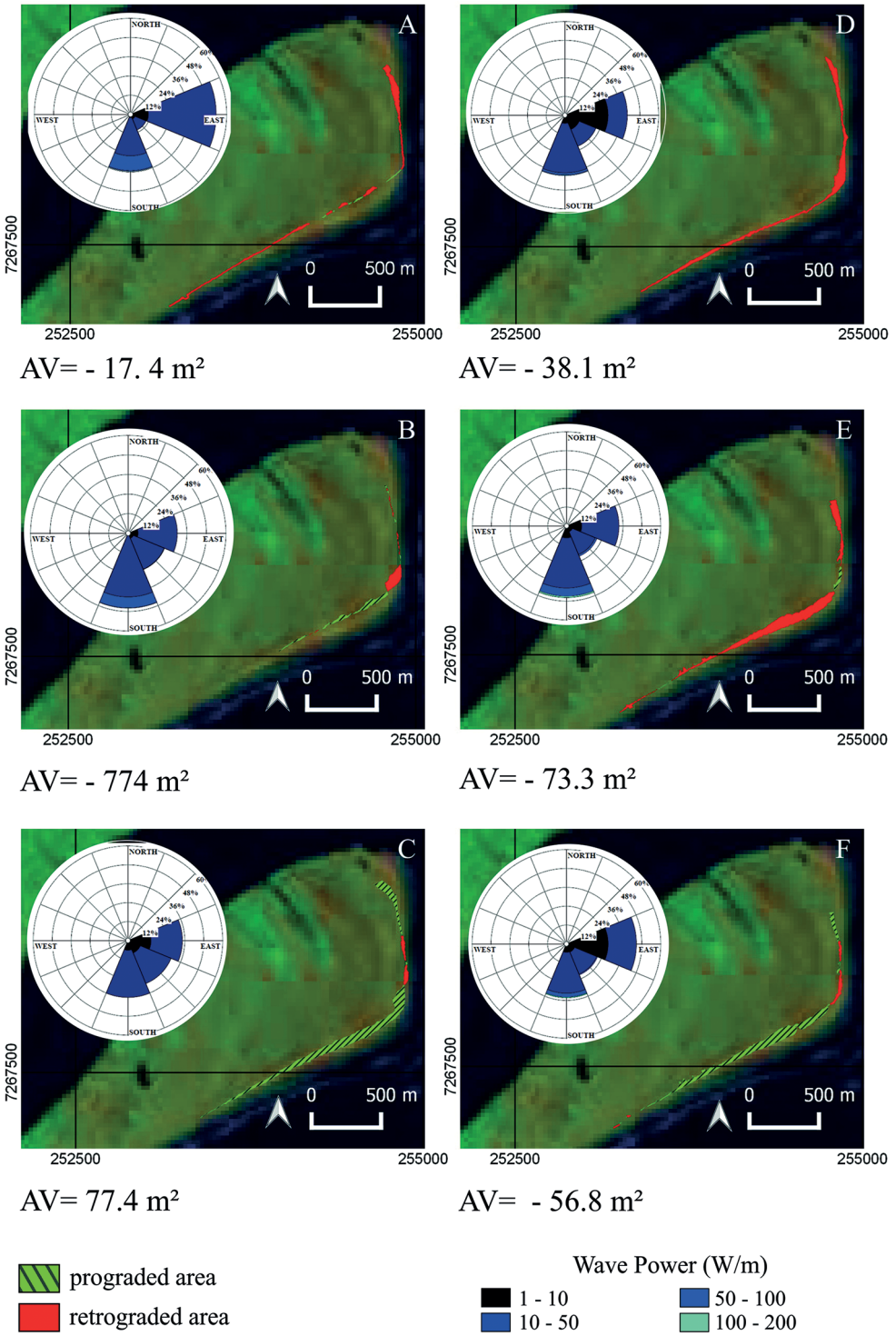

Figure 3. Coastline variations observed with GNSS surveys and area variation (AV). Histograms show wave power (W/m) and preferential wave direction between surveys. (A) Interval I; (B) Interval II; (C) Interval III; (D) Interval IV; (E) Interval V; (F) Interval VI. Image source: Landsat ETM+ from 2017.

observable. Facing the channel, there is an alternation between progradation and retrogradation.

Remote Sensing

Sections from Icapara inlet coastline (I and II) show progradation with rates up to 170 m/y (Figure 4). Sections IV and V show, in general, retrogradation or stable coastlines. Section III showed the highest variability in dynamics, compared to other sections. It is characterized by an initial progradation phase, starting a retrogradation phase after 2005 (Figure 4), probably because of its position between the baymouth and the open sea beaches (Figure 2).

During the analyzed period (1962 to 2017), there was a prevalence of area increase, with a total of $557x10^3$ m^2. However, two different long-term trends were noticed: from 1980 to 2005, the area incrementally increases at a rate of $32x10^3$ m^3/y, whereas from 2006 to 2016, area is lost at a rate of $63x10^3$ m^2/y. Another important morphodynamic feature is that the evolution of the northeastern portion is not linear, showing inter-annual variability due to new beach/dune ridges (incipient foredunes) deposited in the vicinity of the Icapara inlet. These beach/dune ridges are observable in satellite images and in the field with incipient vegetation. They are generally eroded later (Figure 5).

OSL ages

Luminescence signals show very high sensitivity, as previously reported in the region (Sawakuchi et al., 2008). As a consequence, equivalent estimated doses present low errors and low overdispersion (Table 4). Dose rate varied from 0.41 to 0.50 mGy/y, similar to dose rates already described in other studies when referring to the same region (Suguio et al., 1999; Suguio et al., 2003; Sawakuchi et al., 2008; Giannini et al., 2009; Guedes et al. 2011). Rejected aliquots were mostly rejected through a recuperation test (up to 5% limit) and recycling ratio (0.9-1.1), with an acceptance rate of 80% for samples IC62 and IC01, and 58% for sample IC03. Following the same criteria, on the dose recovery test, 80% of sample ICM08 aliquots were approved.

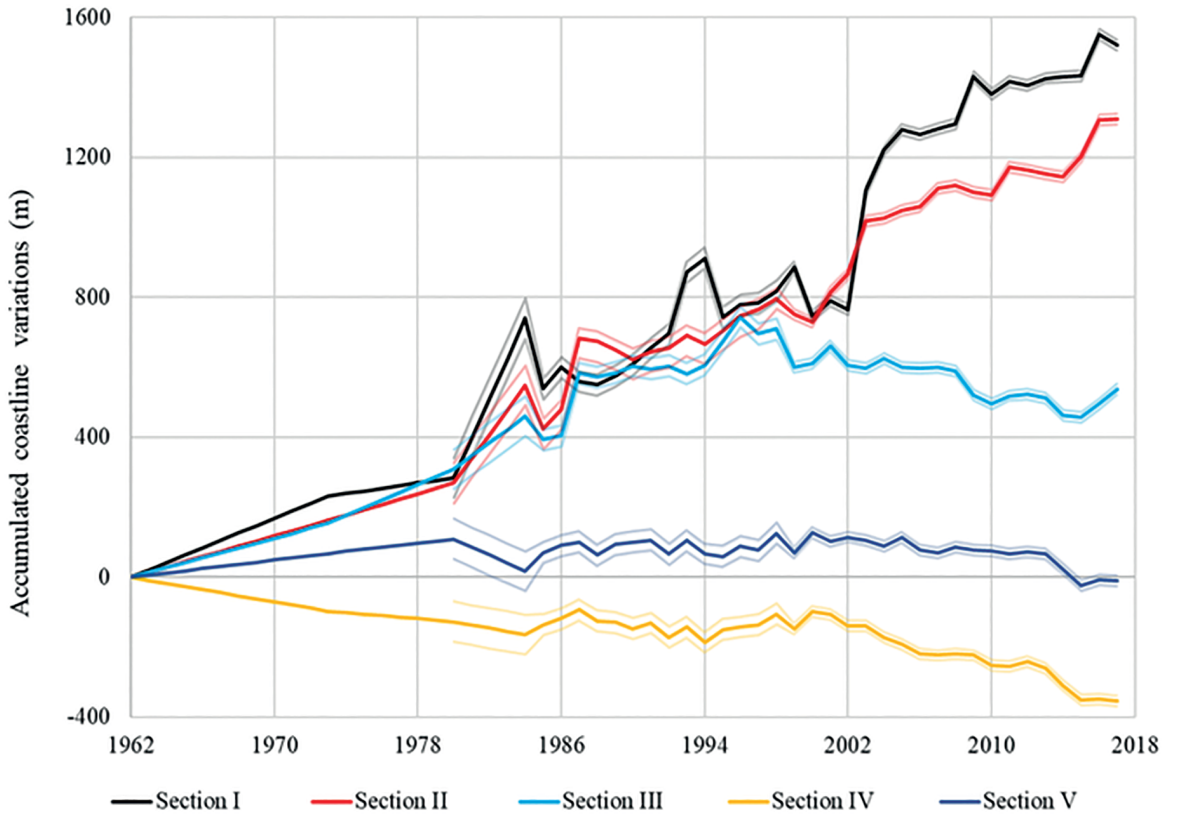

Figure 4. Accumulated coastline variations between 1962 and 2017 years, obtained using aerial photographs and satellite images. Shaded area represents the error associated to image resolution.

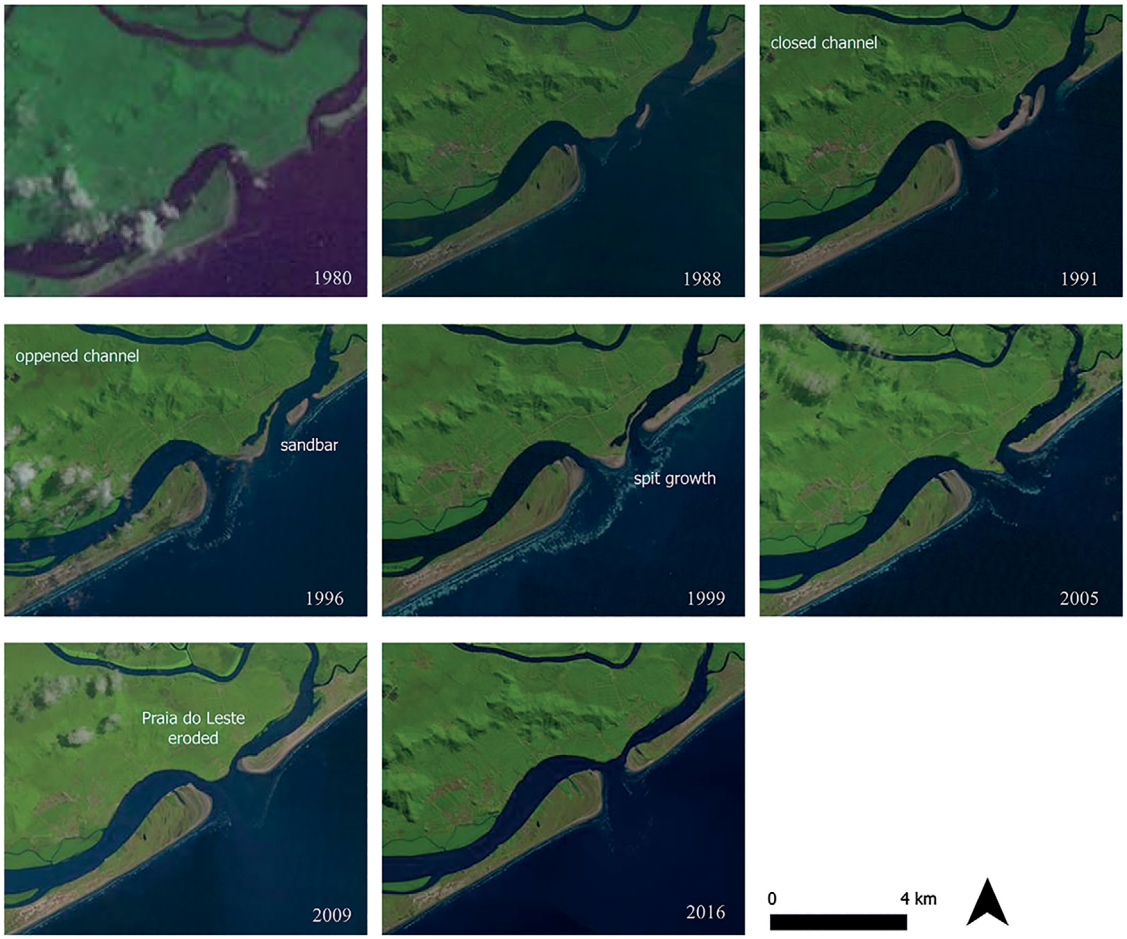

Figure 5. Time-series satellite images of the northeastern stretch of Ilha Comprida, São Paulo, spanning from 1980 to 2016. Source: Satellite image ETM+7 from 2017 obtained from USGS.

Table 4. OSL dating results; x represents aliquots accepted and y the total aliquots analyzed. O.D.: Overdispersion.

Sample	Depth (m)	Number of aliquots (x/y)	Dose (mGy)	O.D. (%)	K (%)	Th (ppm)	U (ppm)	Gamma (mGy/a)	Beta (mGy/y)	Cosmic dose rate (mGy/y)	Dose rate (mGy/y)	Age (y)
ICM08	0	4/5	4.5 ± 1.5	0	0.174 ± 0.02	0.43 ± 0.14	0.34 ± 0.05	0.102 ± 0.01	0.189 ± 0.01	0.1558 ± 0.0078	0.411 ± 0.03	11 ± 4
IC62	0.75	12/15	49.5 ± 3	22 ± 5	0.174 ± 0.02	0.43 ± 0.14	0.34 ± 0.05	0.102 ± 0.01	0.189 ± 0.01	0.1558 ± 0.0078	0.411 ± 0.03	120 ± 11
IC01	0.65	9/12	64.5 ± 4.5	19 ± 5	0.199 ± 0.02	0.89 ± 0.15	0.28 ± 0.05	0.124 ± 0.01	0.211 ± 0.02	0.1558 ± 0.0078	0.436 ± 0.03	148 ± 14
IC03	0.85	7/12	79.5 ± 4.5	12 ± 4	0.304 ± 0.02	0.61 ± 0.14	0.26 ± 0.05	0.134 ± 0.01	0.284 ± 0.02	0.1558 ± 0.0078	0.502 ± 0.03	159 ± 16

Dose recovery tests, performed using 180°C and 200°C preheat temperatures, show satisfactory results in both scenarios (Figure 6), indicative that usage of the SAR protocol is appropriate to estimate the low natural doses expected. However, aliquots with 200°C preheat performed better, having less dispersion of dose recovery results and respecting the limits on the recycling ratio (from 0.92 ± 0.06 to 1.03 ± 0.08) and recuperation tests (1.44 ± 1.54 % to 2.84 ± 0.83 %). A small OSL residual signal was identified on

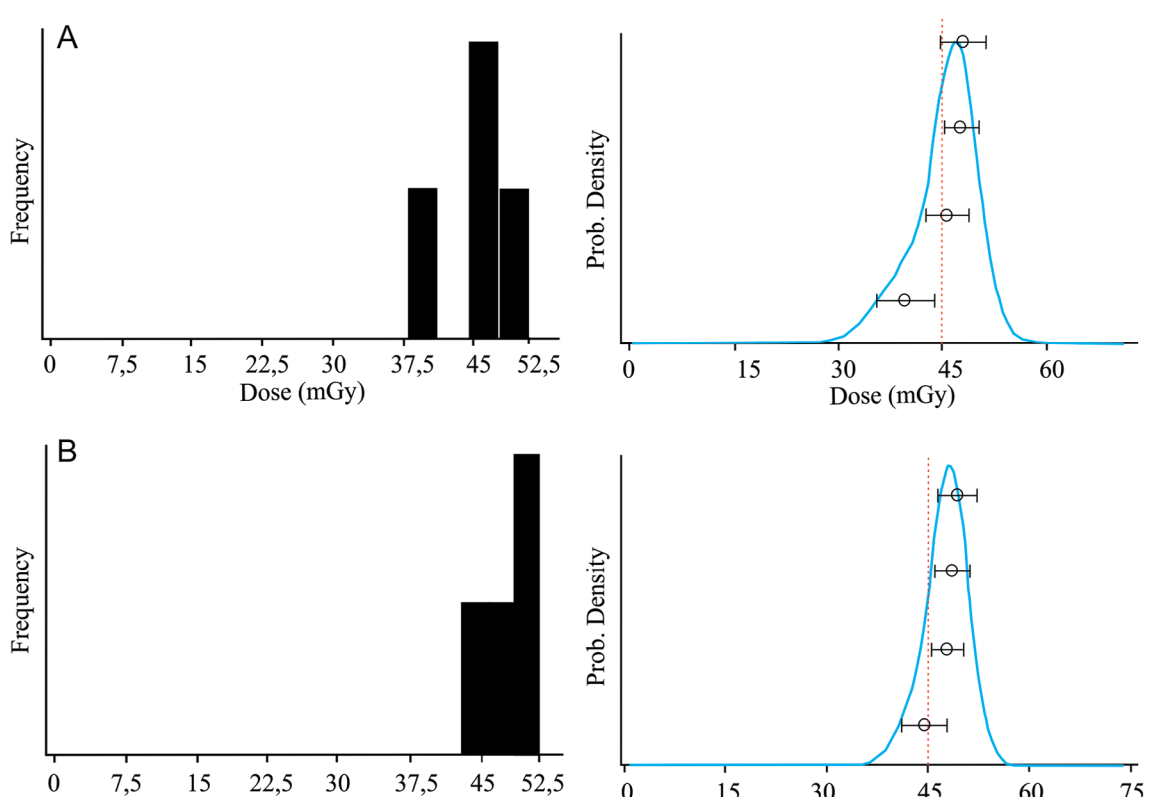

Figure 6. Dose recovery test results for (a): preheat of 180°C and (b) preheat of 200°C. The dotted red line represents the known dose applied.

sample ICM08, from the current beach, resulting in a background age of 11± 4 years. This value is similar to the uncertainty of the OSL ages of the beach ridges.

The OSL age distribution between the beach ridges is geographically coherent; nevertheless, the samples IC01 and IC03 overlap within the error limits. The calculated progradation rates on older beach ridges, considering the age uncertainty and the residual signal, range from 17 to 134 m/y (Figure 7b). As for the most recent beach ridges, the progradation rates range from 9 to 17 m/y.

Climatic dataset

The variability of annual accumulated precipitation, over the studied area, varied from 1100 mm to 2400 mm per year, with a mean of 1716 mm, from 1950 to 2013 (Figure 8). Jun-Jul-Aug were the driest months, whereas Jan-Feb-Mar were the rainiest months, although there has been natural inter-annual variability in the time series (Figure 8). Precipitation above the annual accumulated mean occurs in agreement with some El Niño episodes, from 1980 to 2013, such as in 1982-1983, 1995-1998, 2004-2005 and 2008-2011. During these years, the El Niño (negative SOI values) occurred for several months along the time-series, ranging from weak and strong intensities. Even so, some values below the mean are found in the presence of El Niño episodes (Figure 8).

Average river discharge (from 1940-2016), in the Registro station, is 453 m^3/s (Figure 9), ranging from 282m^3/y (1978) to 889m^3/s (1983). In the Sete Barras station, the mean river flow is 286 m^3/s, with a minimum flow of 162 m^3/s (1985) and maximum of 587 m^3/s, in 1983. Eldorado station records varied from 149 m^3/s (1978) to 530 m^3/s (1983). In agreement with the rainfall regime, lower river flow occurred in the months of Jun-Jul-Aug; and higher flow occurred in Jan-Feb-Mar. Also, like precipitation variability (Figure 8), the highest river flow occurred during El Niño events with strong magnitudes, such as in 1972, 1983, 1992, 1997 and 2015.

Offshore wave distribution indicates some variations in wave regime depending on the season (Figure 10). In all analyzed data, there is a predominance of wave direction from the south (27%) and from the east (24%), with an average peak period of 9.0 seconds and an average

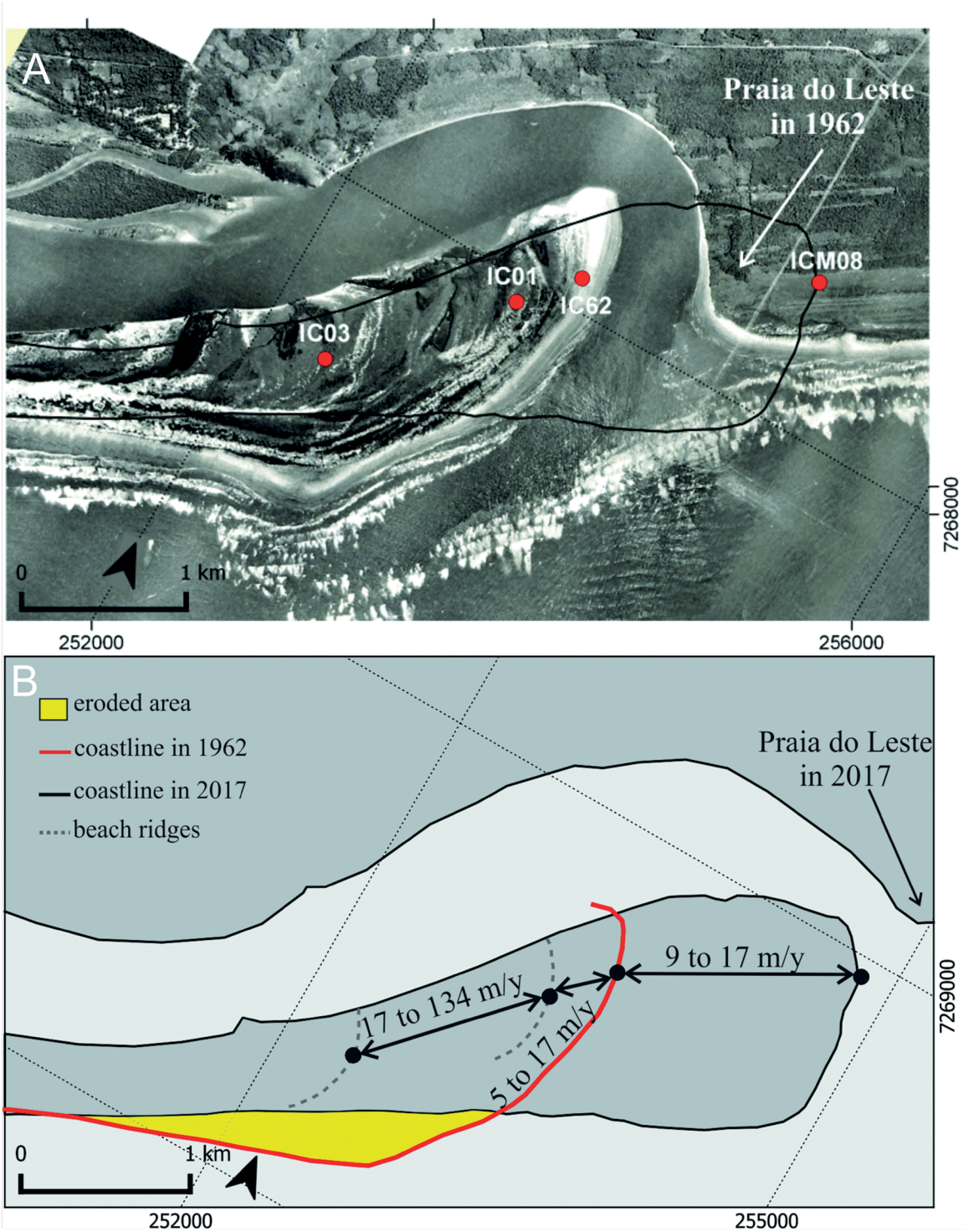

Figure 7. Progradation rates by OSL ages. a) Aerial photography from 1962 with boundary of the coastline in 2016 and sampling points in red. b) Progradation rates between beach ridges. The red line represents the coastline in 1962, while the eroded beaches are in yellow.

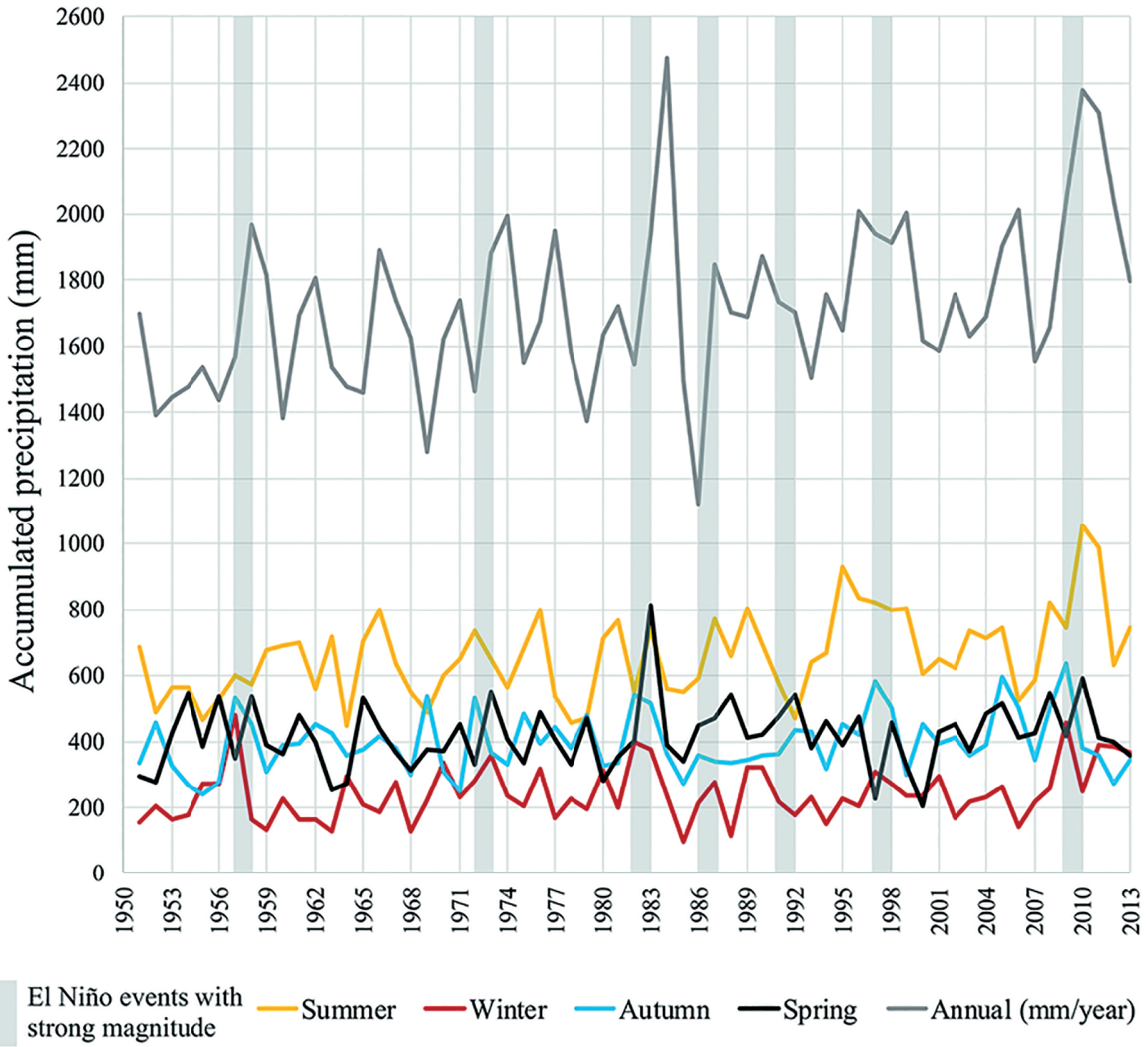

Figure 8. Accumulated and seasonal precipitation over the studied area. The seasons corresponds to the Southern Hemisphere (Sum: DJF; Aut: MAM; Win: JJA; Spr: SON).

height of 1.53 m. The summer and spring seasons have a similar wave regime, with the predominant wave direction from the east (30%) and the south (21%), a climate pattern in the studied region. During the winter, the wave regime is dominated by waves from the south (34%) and from the east (22%), whereas in the autumn the wave predominance is of south (30%) and south-southeast (22%) waves. The highest mean wave heights occur in the winter (4.89 m) and in the autumn (4.73 m); likewise, the same seasons had the highest mean wave power, showing 263 W/m and 248 W/m, respectively. As for the wave peak period, the highest values occurred in the autumn (20.1 seconds) and in the winter (19.3 seconds).

During the intervals of GNSS surveys, the wave regime reflects the seasonal mean. Wave power ranged from 1 to 200 W/m, with a mean of 20.63 W/m and standard deviation of 17.61 W/m (Figure 11). The highest wave power occurred mainly in August; whereas lowest happened in the first trimester. For instance, the summer intervals (III and VI) show the lowest mean height and peak period and, consequently, the lowest wave power (Figure 3). Furthermore, although the frequency of east waves is higher in some intervals (I, III and VI), the wave power from south waves was always stronger than east ones (Figure 10).

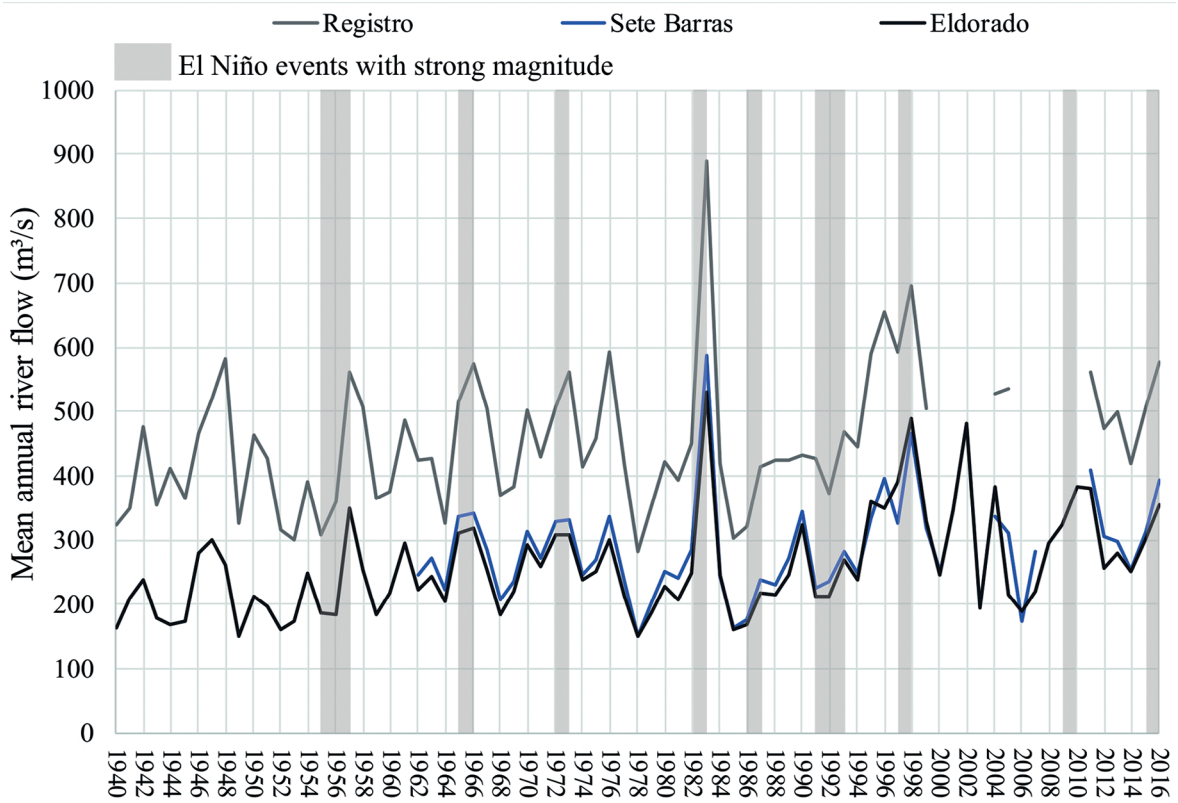

Figure 9. Mean annual river flow (m^3/s) at Registro, Sete Barras and Eldorado stations.

DISCUSSION

The natural dynamics prior to the channel opening

Most other studies on Ilha Comprida's growth pattern correlate it to Valo Grande, but usually analyze the dynamics after the channel opening event (Table 5). Studies such as Guedes et al. (2011a) and Pimentel (1762) detected similar growth rates in periods before anthropogenic interference. For the most recein nt beach ridges, the rates are very similar to the growth pattern of the island in the last 6000 years, as described by Guedes et al. (2011a). From 6000 to 5000 years ago, the area increased at rates of $55x10^3$ m^2/y; then, rates decreased to $10x10^3$ m^2/y, until about 2000 years ago. During this period, the morphodynamic had no influence from Icapara Hill or Valo Grande. Furthermore, it comprises a longer interval of time, compared to others time intervals, probably being influenced by long-term variations. Also, this time interval is reported to be less favorable to channel migration, with less storm activity (Sawakuchi et al. 2008, 2012).

In this study, the same dynamic of formation of curved beach ridges at the northeastern end of the island, maintaining the hook shape over the last 6000 years, was observable (Guedes et al., 2011a). Curved beach ridges are formed through the addition of sediments into northeastern end beaches, while erosion occurs on the other side of the channel. The Valo Grande channel opening favored the trapping of coastal sediments in the barrier system due to the intensification of the hydraulic jetty of the Icapara Inlet (Guedes et al., 2011a).

Silva et al., (2016) indicates the variation of potential longshore drift, direction and intensity, regarding a seasonal distribution of the 30-year wave dataset from WW3®, corroborating the results obtained by Nascimento et al. (2008), Giannini et al. (2009) and Guedes et al. (2011b) showing a bidirectional potential longshore drift. Guedes et al. (2011b), using grain-size and heavy minerals analysis, suggested the northward predominance of coastal drift at the NE end of the IC barrier throughout the evolutionary history of the island.

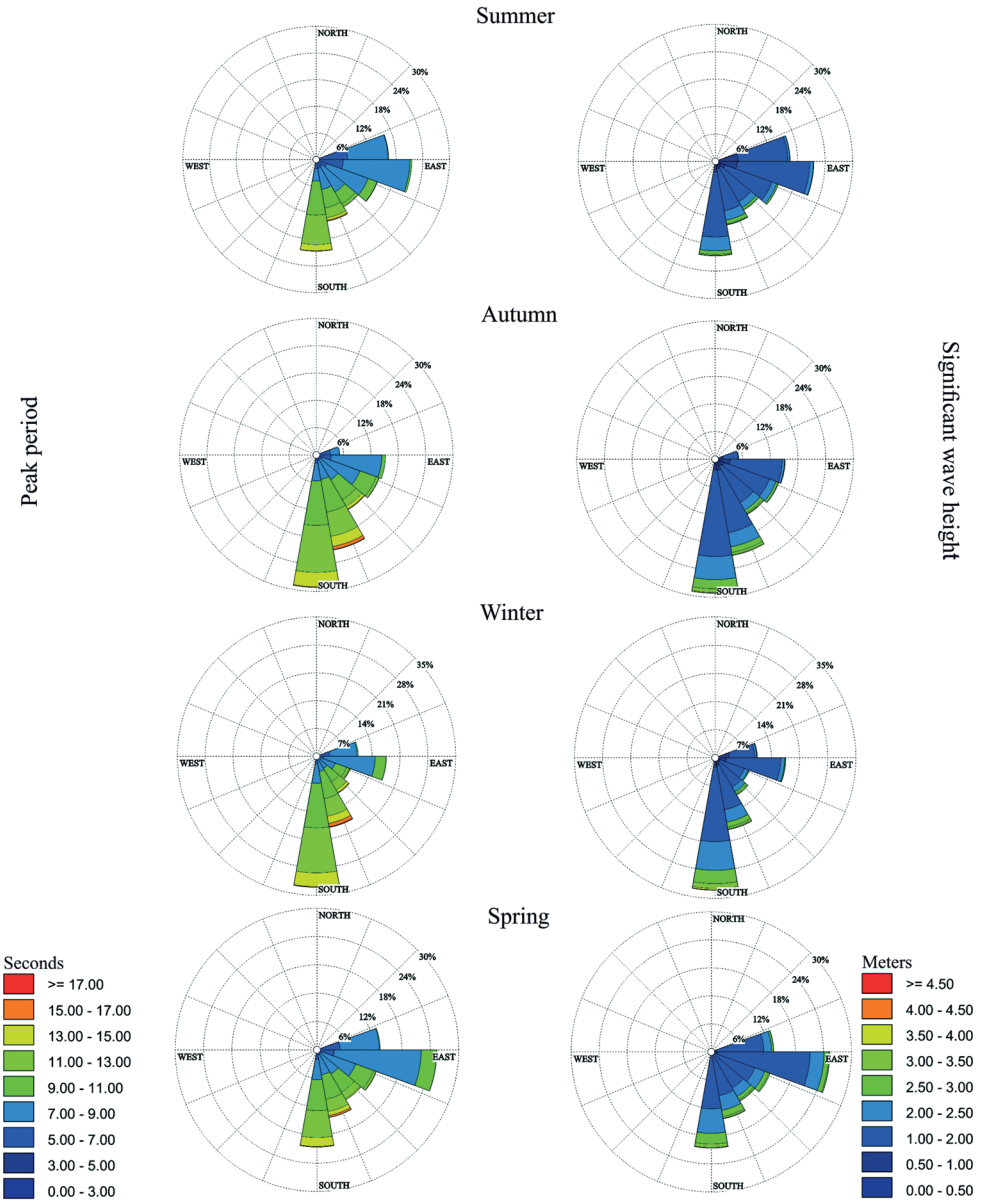

Figure 10. Seasonal wave regime from 1979 to 2017. Direction, peak period and significant wave height. The seasons correspond to Southern Hemisphere (Sum: DJF; Aut: MAM; Win: JJA; Spr: SON).

The comparison between the northeastward growth rates from millennial to annual time scales indicated acceleration in the growth of beach ridges. There is a growth rate between 36 and 154 m/y just before the Valo Grande opening, from 222±23 (sample ICL-9C from Guedes et al., 2011a) and 159±16 (IC03). This period coincides with the last years of the Little Ice Age (LIA). The higher frequency and/or intensity of cold fronts caused erosional conditions on the coast (Sawakuchi et al., 2008). Thus, the acceleration of dynamics in the IC is also influenced by climate, besides anthropogenic influences, altering the interaction between these agents.

The anthropogenic influence on natural systems: the case of the Valo Grande opening

Double-frequency GNSS surveys allow more detailed analysis of the dynamics of the coastline. The relationship of the dynamics of the Icapara inlet is commonly related to local factors, such as the river

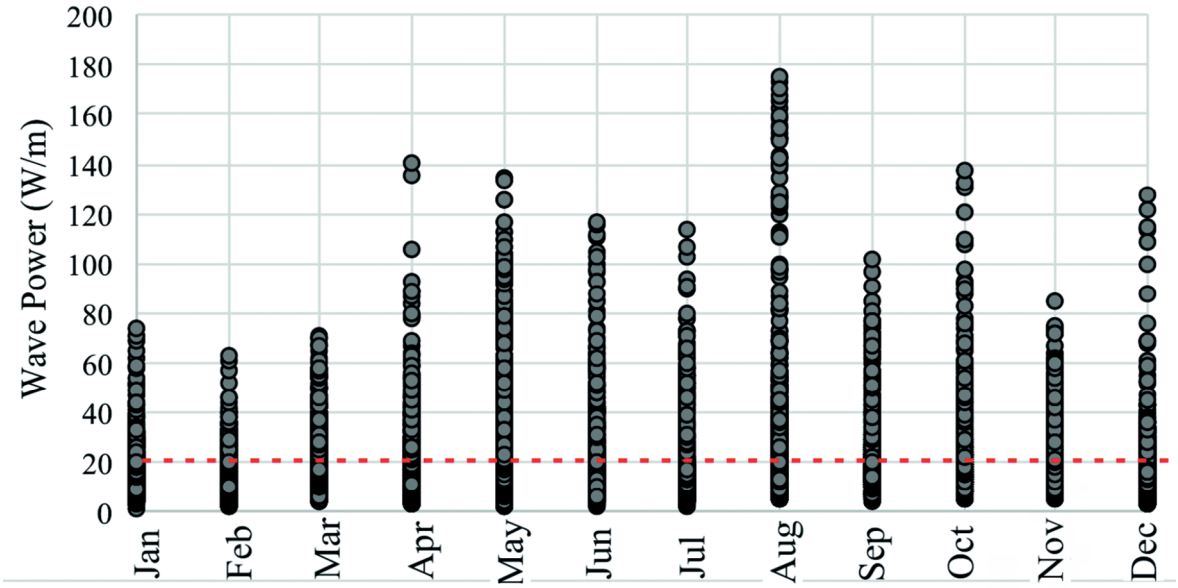

Figure 11. Ratio between wave power and its monthly occurrence from 2015 to 2017. Dotted red line is the mean wave power for the period.

Table 5. Ilha Comprida island northeastward growth rates obtained from previous studies and the present study.

Migration rates (m/y)	Period	Method (s)	Source
15.5	May/15 to Mar/17 AD	GNSS surveying	This study
32	1980 to 2016 AD	Satellite images and aerial photos	This study
27.7	1976 to 2013 AD	Satellite images	Alcántara-Carrió *et al*. (2017)
15.5	1976 to 2000 AD	Satellite images	Kawabuko (2009)
27.5	1962 to 2000 AD	Aerial photos	Nascimento *et al*. (2008)
25 - 30	1810 to 2010 AD	OSL ages	Guedes *et al*. (2011)
35	1882 to 1964 AD	Old maps and aerial photos	Geobras (1966)
5 - 134	1840 to 1906 AD	OSL ages	This study
19.3	1721 to 1882 AD	Old maps	Pimentel (1762) and Alcántara-Carrió *et al*. (2017)
5 - 7	4800 to 2000 years ago	OSL ages	Guedes *et al*. (2011)
10 - 23	6000 to 4800 years ago	OSL ages	Guedes *et al*. (2011)
8	6000 to 2000 years ago	OSL ages	Guedes *et al*. (2011)

flow of the Ribeira de Iguape and Valo Grande, the potential longshore drift, and the wave and wind regime (Geobrás, 1966; Nascimento et al., 2008; Kawakubo, 2009; Silva et al., 2016; Alcántara-Carrió et al., 2017). Northeastward migration rates from the IC obtained in this study ranged from 15.5 m/y, in the GNSS surveys, to 134 m/y, calculated from OSL rates. The range of the migration rates is in accordance with many progradation rates calculated by others authors over different time scales and with different methods (Table 5).

Ages obtained from samples IC03 and IC01 are associated with the period of construction and opening of the artificial channel of Valo Grande (between 1841 and 1882). This period is related to the moment of greatest erosion in the channel, between 1875 and 1890 (Young, 1903; Geobrás 1966; Furtado et al., 1981; Nascimento et al. 2008), which elevated the volume of sediments carried to the lagoon and the beach, and may be determinant for the high rates of island migration. This fact corroborates with Nascimento et al. (2008) and Alcántara-Carrió et al. (2017), regarding

the acceleration in migration rates during the channel's enlargement. Indeed, the island's accretion rate has increased from $35x10^3$ m^2 per year (from 2.0 to 0.2 ka B.P., Guedes et al., 2011a) to $90x10^3$ m^2 per year, after the end of the blockade by the hills near Iguape and the opening of the Valo Grande (Guedes et al., 2011a). These high rates, however, have occurred over the last few decades. From 1980 to 2008, there was a rate of $43x10^3$ m^2 per year, followed by a rate of $-37x10^3$ m^2, resulting in an erosional period that lasted until 2017. Thus, despite the anthropogenic interference made by the Valo Grande opening on the inlet, dynamics have been almost continuous; these interferences seem to have more of an effect on the system disturbance during its beginning.

The climate anomalies causing the intensification or reduction of rainfall modify the patterns of the controlling mechanisms of coastal systems (Viles and Goudie, 2003; Barnard et al., 2017; Carvalho et al., 2020). The beach ridges developed during the El Niño of 1983 resulted in a net growth in area until 1986. Furthermore, there was an emergence of sand banks eroding from Praia do Leste related to higher river flows. A new spit formed in 1989 and migrated to Icapara Inlet in 1999-2000 (Figure 5) due to the dominant northeastward longshore drift. This short period (1989 to 1999) has the influence of three intense El Niño events that propitiated the formation and degradation of the first baymouth spits (Figure 5 and 12).

River flow has a moderate to strong correlation with precipitation ($0.4 < R^2 < 0.7$) at three stations (Figure 13). The precipitation explains 69% of the variability of the river flow over the Registro station, which is the most representative of Valo Grande's flow due to its location. Also, it is observed that some precipitation and river flow anomalies are coincident with El Niño events (Figures 8 and 9). This implies that the monitoring of the Valo Grande flow according the climate variability is an important management tool for the many activities that depend on this channel.

During the first closing episode of Valo Grande, the occurrence of El Niño was associated with above mean precipitation on the region, which induced the dam to rupture in 1983 (Figure 12, Souza et al., 2016). After this climatic anomaly, the driest period in series occurred in 1985. Between 1985 and 1992, the river flow was less intense in comparison to previous periods. However, the barrier has grown $790x10^3$ m^2. This period is marked by major morphological changes due to the intense erosion on Jureia beach spit (until 1988), contributing with the reorganization of eroded sediments at the northeastern end of the island. Coastline prograded mainly in sections II and III, closest to the spit. The increase and decrease of area in this period were probably controlled by variations in wave power.

After 1988, eroded sediments from Praia do Leste formed sand banks, which are associated with the trend of increased river flow since 1992 (Figure 14). Its northeastward migration caused by longshore drift resulted in the progradation of the Jureia beach spit, forming a baymouth spit. Between 1991-1998, the area variation becomes more stable even with an increase of precipitation and river flow until 1998. This stability is probably due to the construction and closure of the channel dam (1990 - 1995), that reduced the flow of sediments in the Mar Pequeno lagoon and the inlet dynamics. With the opening of the channel, the high river flow through the inlet eroded the sediment from the beaches (on sections II and III), resulting in a negative balance in 1998 (Figure 5 and 12).

The Praia do Leste beach was almost entirely eroded in 2005. Is possible to observe, in satellite images, intratidal sand banks merging during this year (Figure 5); this may have contributed to the increase of area on the northeastern end of the island. The coastline prograded more than 100 m in all sections located at the baymouth beaches (Figure 4) and, from that period to present, there is a tendency of decreasing in the area as a whole (Figure 12a).

In 2009, the Praia do Leste beach eroded completely and resulted in a flanking baymouth spit between the river mouth and the Icapara inlet (Figure 5), as verified by Alcantára-Carrió et al. (2017). Even with the El Niño favoring above mean precipitation and above mean flow rates, the area exhibits a decreasing trend (Figure 12). In this period, there were changes in coastline directions following the river flow, which exhibits similarities with the actual morphology. River discharge acts as hydraulic blockage causing changes in the wave pattern that influence the coast. With the preferential drift heading northeast along with a hydraulic blockage, the coastline at the open sea beaches (Sections IV and V) became exposed, throughout the year, to waves with erosive

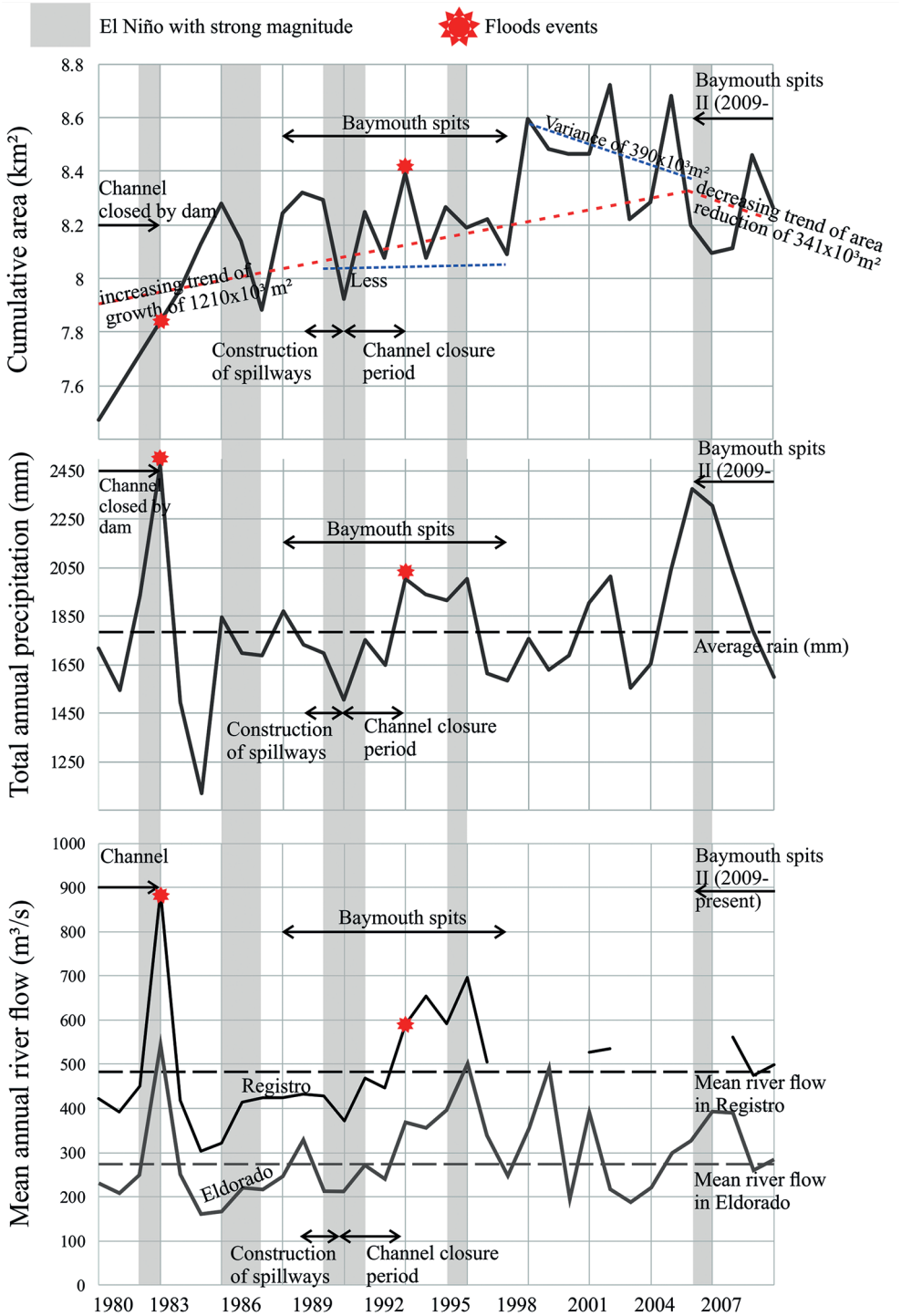

Figure 12. Annual variation of a) accumulated area; b) accumulated precipitation and c) mean river flow in each one of the stations. Gray bars represent time-intervals of El Niño with strong magnitude events. Arrows indicate time-interval of events and disturbances in the system. Red points mark flood events at Valo Grande.

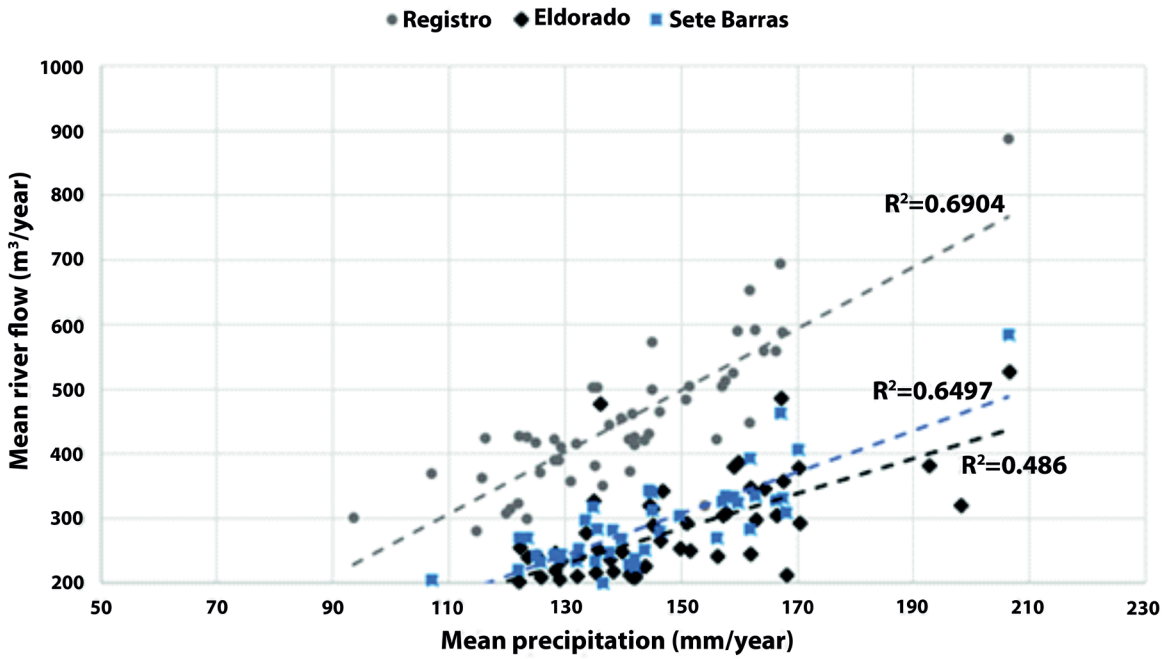

Figure 13. Scatter plot showing the relationship between between mean annual precipitation and mean annual river flow in Registro, Sete Barras and Eldorado stations.

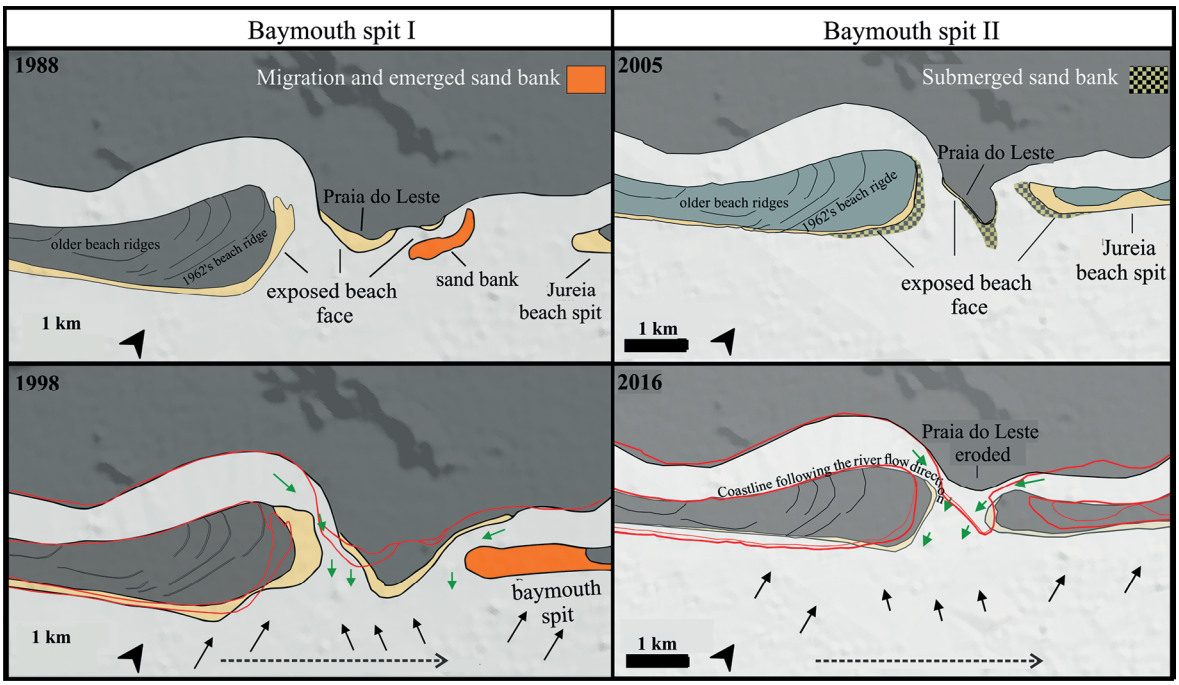

Figure 14. Baymouth spit formation and evolution. The first event (1988 to 1998) is marked for migration and emergence of a sand bank at the Juréia beach spit and high progradation at the baymouth beach of Ilha Comprida, with punctual erosion in such a way that the southern waves seem to affect the coastline. In the second event (2005 until present), erosive processes removed all sediments from the beach face in Praia do Leste. Also, there was retrogradation on the coastline and the open sea beaches in the island. Green arrows represent river flow; black arrows represent incidence of the southern waves; and the gray arrow is the longshore drift.

character, mainly southern waves, as indicated by Alcantára-Carrió et al. (2017) and Silva et al. (2016).

Silva et al. (2016) indicated that during the winter and the autumn, the resulting potential longshore drift is northeastward, with the highest potential during winter (Figure 15b and c), whereas in the spring and in the summer, the resulting drift is southwestward, with greater potential in the spring (Figure 15a and d). Also, the resulting potential longshore northeastward drift, over the northeast coastal area of the island, contributes with an intense erosive character, as previously characterized by Souza and Suguio (1996). This erosive phase is observable mainly in the winter, due to lower river flow and higher wave power, from the south, with erosive behavior (Figure 9), as also noted by Sawakuchi et al. (2008) in beach ridge patterns during the Little Ice Age (LIA). Even over different time scales, the erosive processes have intensified, following the south waves.

The opposite configuration occurs during the summer (Figure 15a). After that, the headland erosion merged the river mouth and the Icapara inlet, in 2009, acting as a hydraulic blockage for longshore drift (Alcantára-Carrió et al., 2017). Previously, there was a predominance of tidal currents in the flow control of the Icapara inlet (Bonetti-Filho et al., 1996) but the sediments transported by the coastal drift were blocked by the effect of hydraulic jetty caused by the discharge of water from the Icapara mouth (Geobrás, 1966; Nascimento et al., 2008). During the GNSS surveys, the Icapara mouth had already merged with the river mouth, favoring the drift blockage in proportion to the river flow and changing the wave incidence pattern.

CONCLUSIONS

Although the region is remotely influenced by anomalies, such as El Niño events, the anthropogenic influence on barrier evolution was the focus of the study. The impact of anthropogenic influence can be characterized by increasing rates of coastline progradation near the spit during the enlargement of the Valo Grande artificial channel.

The interaction between climatic agents is determinant on sediments dispersion, influencing progradation and erosion rates. The Valo Grande channel has contributed to sediment retention by the hydraulic jetty. The blockage occasioned by river

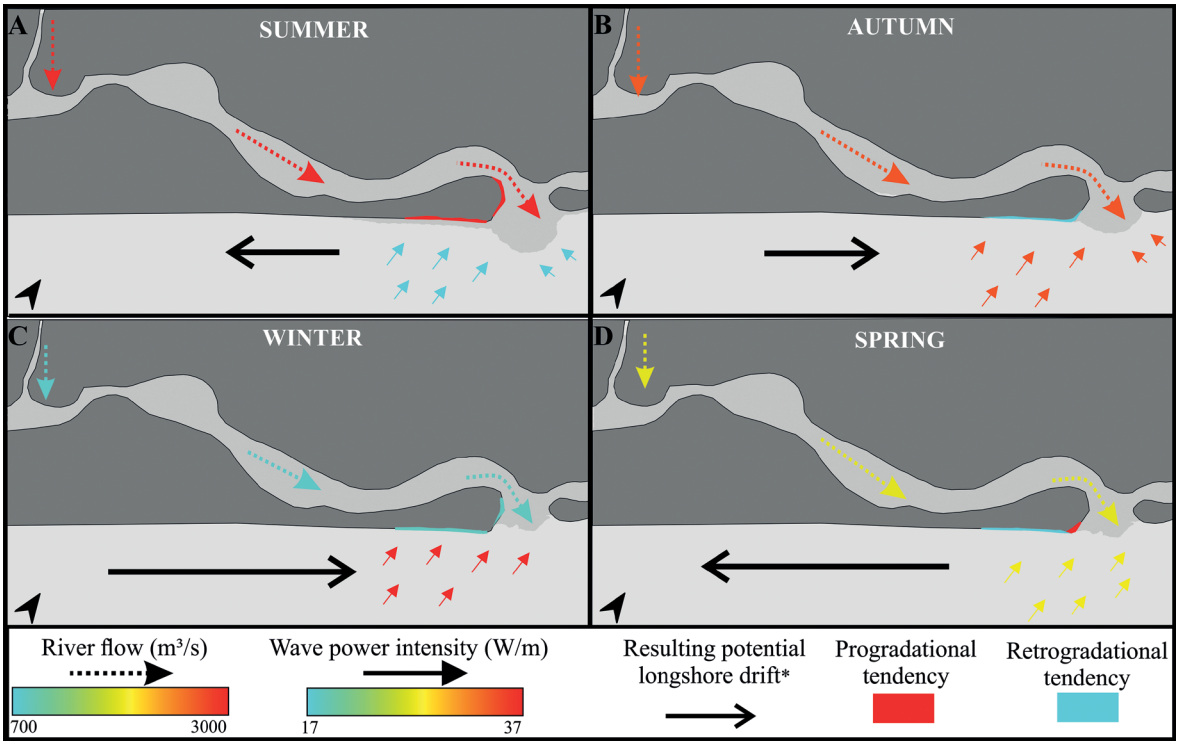

Figure 15. Conceptual model to seasonal morphodynamic. *Resulting potential longshore drift by Silva et al. (2016).

discharge resulted in an increase of the barrier area, mainly on baymouth beach - following the dominant northeastward longshore drift. However, the coastline is exposed to erosive events during most of the year, since the blockade is effective only during the summer. Erosive wave conditions are related to a higher frequency of cold fronts that are associated with intense winds from the southeast and changes the configuration of the beaches. This configuration represents the current morphodynamic state and explains the loss of area on the northeastern end of the island since 2005. The closing of the artificial channel of Valo Grande can cause greater changes in the morphodynamics, interfering in the hydraulic blockade and causing acceleration in the erosive processes of the northeastern end of the barrier island. Coastal instabilities must be alert due to urban growth and expansion of coastal zone urbanization.

Further dynamics analyses are necessary to investigate the inter-annual to decadal mechanisms of natural variability that influence the morphodynamics of the Northeast of Ilha Comprida and some relationships with anthropogenic forces. Ilha Comprida is influenced by the moisture transport during the mature phase of South America's Monsoon System, which, in turn, has its position modified by ENSO-variability. This configuration interferes in rainfall regime and, consequently, with the river flow of the Ribeira de Iguape. It is also possible that the progradation results obtained in this study are related to the displacement of extratopical cyclones over the Ilha Comprida region; further study is needed to focus on a qualitative approach to this relationship.

ACKNOWLEDGMENTS

We would like to thank Eduardo Siegle for the help in obtaining the WW3 data and the Laboratory of Gamma Spectrometry and Luminescence from University of São Paulo/Brazil for OSL dating. This research was founded by National Council for Scientific and Technological Development of Brazil– CNPq (Project 444836/2014-4). We would like to thank the two anonymous reviewers who provided constructive and critical remarks on the manuscript.

AUTHOR CONTRIBUTIONS

M.S.S.: Writing - original draft; Writing - review & editing;

C.C.F.G.: Investigation; Supervision; Writing - review & editing;

G.A.M.S.: Investigation; Writing - review & editing; G.P.R.: Investigation; Methodology.

REFERENCES

ALCÁNTARA-CARRIÓ, J., DINKEL, T. M., PORTZ L. & MAHIQUES, M. M. 2017. Two new conceptual models for the formation and degradation of baymouth spits by longshore drift and fluvial discharge (Iguape, SE Brazil). *Earth Surface Process and Landforms,* 43(3), 695-709.

AMBROSIO, B. G., SOUSA, P. H. G. O., GAGLIARDI, M. H. & SIEGLE, E. 2020 Wave energy distribution at inlet channel margins as a function of ebb tidal delta morphology: Cananéia Inlet, São Paulo, Brazil. *Anais da Academia Brasileira de Ciências,* 92(1), e20180677.

BARNARD, P. L., HOOVER, D., HUBBARD, D. M., SNYDER, A., LUDKA, B. C., ALLAN, J., KAMINSKY, G. M., RUGGIERO, P., GALLIEN, T. W., GABEL, L., MCCANDLESS, D., WEINER, H. M., COHN, N., ANDERSON, D. L. & SERAFIN, K. A. 2017. Extreme oceanographic forcing and coastal response due to the 2015-2016 El Niño. *Nature Communications,* 8, 14365, DOI: https://doi.org/10.1038/ncomms14365

BASTOS, C. C. & FERREIRA, N. J. 2000. Análise climatológica da alta subtropical do Atlântico Sul. *CEP,* 12220(110), 973-990.

BONETTI-FILHO, J., CONTI, L. A. & FURTADO, V. V. 1996. Suspended sediment concentration variability and its relation to tidal currents in microtidal systems. *Anais da Academia Brasileira de Ciência,* 68(3), 485-494.

CARVALHO, B. C., DALBOSCO, A. L. & GUERRA, J. V. 2020. Shoreline position change and the relationship to annual and interannual meteo-oceanographic conditions in Southeastern Brazil. *Estuarine, Coastal and Shelf Science,* 235, 106582.

CARVALHO, L., JONES, C. & LIEBMANN, B. 2004. The South Atlantic Convergence Zone: intensity, form, persistence, and relationships with intraseasonal to interannual activity and extreme rainfall. *Journal of Climate,* 17(1), 88-108.

CAUS JUNIOR, C. 2010. *Breve estudo sobre a situação fundiária e registraria da comarca de Iguape - SP.* Iguape: Oficial de Registro de Imóveis, títulos e documentos e registro civil de pessoas jurídicas da comarca de Iguape - SP.

CUNNINGHAM, A. C. & WALLINGA, J. 2010. Selection of integration time intervals for quartz OSL decay curves. *Quaternary Geochronology,* 5(6), 657-666.

DAVIDSON-ARNOTT, R. 2010. *Introduction to coastal processes and geomorphology.* Cambridge: Cambridge University Press.

DIAS, J. A. 2005. Evolução da zona costeira portuguesa: forçamentos antrópicos e naturais. *Tourism and Management Studies,* 1, 7-27.

FURTADO, J. S., YAMANAKA, N. & OLIVEIRA, M. C. 1981. *Percepção ambiental e quadro referencial do complexo "Valo Grande e Sistema Lagunar Cananéia-Iguape"* [online]. São Paulo: Secretaria da Agricultura, Coordenadoria da Pesquisa de Recursos Naturais. Available at: http://ftp.sp.gov.br/ftppesca/sumula.pdf.

GEOBRÁS. 1966. *Complexo Valo Grande, Mar Pequeno e Rio Ribeira de Iguape*. Iguape: Engenharia e Fundações S/A – Departamento de Águas e Energia Elétrica.

GIANNINI, P. C. F., GUEDES, C. C. F., ASSINE, M. L., ANGULO, R. J., SOUZA, M. C., PESSENDA, L. C. & TATUMI, S. H. 2003. *Variação transversal e longitudinal de propriedades sedimentológicas nos cordões litorâneos da ilha Comprida, litoral sul paulista. In:* IX ABEQUA (Congresso da Associação Brasileira de Estudos do Quaternário). Recife, PE, October 12-19, 2003, ABEQUA, Recife, pp. 288.

GIANNINI, P. C. F., GUEDES, C. C. F., NASCIMENTO JUNIOR, D. R., TANAKA, A. P., ANGULO, R. J., SOUZA, M. C. & ASSINE, M. L. 2009. Sedimentology and morphological evolution of the Ilha Comprida barrier system, southern São Paulo coast. *In:* DILLENBURG, S. R. & HESP, P. A. (eds.). Geology and geomorphology of Holocene coastal barriers of Brazil. Berlin: Springer-Verlag, pp. 177-224.

GOODWIN, I. D., STABLES, M. A. & OLLEY, J. M. 2006. Wave climate, sand budget and shoreline alignment evolution of the Iluka-Woody Bay sand barrier, northern New South Wales, Australia, since 3000 yr BP. *Marine Geology,* 226(1-2), 127-144.

GUEDES, C. C. F., GIANNINI, P. C. F., NASCIMENTO JUNIOR, D. R., SAWAKUCHI, A. O., TANAKA, A. P. B. & ROSSI, M. G. 2011b. Controls of heavy minerals and grain size in a Holocene regressive barrier (Ilha Comprida, southeastern Brazil). *Journal of South American Earth Sciences,* 31(1), 110-123.

GUEDES, C. C. F., GIANNINI, P. C. F., SAWAKUCHI JUNIOR, A. O., DEWITT, R., NASCIMENTO JUNIOR, D. R., AGUIAR, V. A. P. & ROSSI, M. G. 2011b. Determination of controls on Holocene barrier progradation through application of OSL dating: the Ilha Comprida Barrier example, Southeastern Brazil. *Marine Geology*, 285(1-4), 1-16.

GUEDES, C. C. F., SAWAKUCHI, A. O., GIANNINI, P. C. F., DEWITT, R. & AGUIAR, V. A. P. 2013. Luminescence characteristics of quartz from Brazilian sediments and constraints and constraints for OSL dating. *Anais da Academia Brasileira de Ciências,* 85(4), 1303-1316.

HEMER, M. A., CHURCH, J. A. & HUNTER, J. R. 2010. Variability and trends in the directional wave climate of the Southern Hemisphere. *International Journal of Climatology,* 30(4), 475-491.

HERRERO, X., COSTAS, S. & KOMBIADOU, K. 2020. Coastal ridge constructive processes at a multi-decadal scale in Barreta Island (southern Portugal). *Earth Surface Processes and Landforms,* 45(2), 411-423.

KANAMITSU, M., EBISUZAKI, W., WOOLLEN, J., YANG, S. K., HNILO, J. J., FIORINO, M. & POTTER, G. L. 2002. CEP-DOE AMIP-II reanalysis (R-2). *Bulletin of the American Meteorological Society,* 83, 1631-1643.

KAWAKUBO, F. S. 2009. Avaliação das mudanças na linha de costa na foz do rio Ribeira de Iguape/desembocaura lagunar da Barra do Icapara (litoral sul de São Paulo-Brasil) utilizando dados do Landsat MSS, TM e ETM+. *Investigaciones Geográficas (Mx),* 68, 41-49.

KILADIS, G. N. & VAN LOON, H. 1988. The Southern Oscillation. Part VII: Meteorological anomalies over the Indian and Pacific sectors associated with the extremes of the oscillation. *Monthly Weather Review,* 116(1), 120-136.

MAHIQUES, M. M., BURONE, L., FIGUEIRA, R. C. L., LAVENÉRE, W., ANDERLEY, A. A. O., CAPELLARI, B., ROGACHESKI, E. C., BARROSO, C. P., SANTOS, A. L. S., CORDERO, L. M. & CUSSIOLI, M. C. 2009. Anthropogenic influences in a lagoonal environment: a multiproxy approach at the Valo Grande mouth, Cananéia-Iguape System (SE Brazil). *Brazilian Journal of Oceanography,* 57, 325-337.

MAHIQUES, M. M., FIGUEIRA, R. C. L., ALVES, D. P. V., ITALIANI, D. M., MARTINS, C. C. & DIAS, J. M. A. 2014. Coastline changes and sedimentation related with the opening of an artificial channel: the Valo Grande Delta, SE Brazil. *Anais da Academia Brasileira de Ciências,* 86(4), 1597-1607.

MAHIQUES, M. M., FIGUEIRA, R. C. L., SALAROLI, A. B., ALVES, D. P. V. & GONÇALVES, C. 2012. 150 years of anthropogenic metal input in a biosphere reserve: the case study of the Cananéia-Iguape coastal system, Southeastern Brazil. *Environmental Earth Sciences,* 68(4), 1073-1087, DOI: https://doi.org/10.1007/s12665-012-1809-6

MARENGO, J. A., SOARES W. R., SAULO, C. & NICOLINI, M. 2004. Climatology of the low-level jet east of the Andes as derived from the NCEP reanalyzes. *Journal of Climate,* 17(12), 2261-2280.

MASSELINK, G., HUGHES, M. & KNIGHT, J. 2014. *An introduction to coastal processes and geomorphology*. Boca Raton: Routledge & CRC Press.

MESQUITA, A. R. & HARARI, J. 1983. Tides and tide gauges of Cananéia and Ubatuba-Brazil (lat. 24). *Relatório interno do Instituto Oceanográfico,* 11, 1-14.

MURRAY, A. S. & WINTLE, A. G. 2000. Luminescence dating of quartz using an improved single-aliquot regenerative-dose protocol. *Radiation Measurements,* 32(1), 57-73.

MURRAY-WALLACE, C. V., BANERJEE, R. P., BOURMAN, J. M., OLLEY, J. M. & BROOKE, B. P. 2002. Optically stimulated luminescence dating of Holocene relict foredunes, Guichen Bay, South Australia. *Quaternary Science Review,* 21(8-9), 1077-1086.

NASCIMENTO JUNIOR, D. R., GIANNINI, P. C. F., TANAKA, A. P. B. & GUEDES, C. C. F. 2008. Mudanças morfológicas da extremidade NE da Ilha Comprida (SP) nos últimos dois séculos. *Geologia USP. Série Científica,* 8(1), 25-39. DOI: http://dx.doi.org/10.5327/z1519-874x2008000100003

NIELSEN, A., MURRAY, A. S., PEJRUP, M. & ELBERLING, B. 2006. Optically stimulated luminescence dating of a Holocene beach ridge plain in Northern Jutland, Denmark. *Quaternary Geochronology,* 1(4), 305-312.

NIMER, E. 1989. *Climatologia do Brasil.* Rio de Janeiro: IBGE.

NOGUÉS-PAEGLE, J. & MO, K. C. 1997. Alternating wet and dry conditions over South America during summer. *Monthly Weather Review,* 125(2), 279-291.

OLLERHEAD, J. & DAVIDSON-ARNOTT, R. G. D. 1995. The evolution of Buctouche Spit, New Brunswick, Canada. *Marine Geology,* 124(1-4), 215-236.

OTVOS, E. G. 2000. Beach ridges - definitions and significance. *Geomorphology,* 32(1-2), 83-108.

PEREIRA, N. E. S. & KLUMB-OLIVEIRA, L. A. 2015. Analysis of the influence of ENSO phenomena on wave climate on the central coastal zone of Rio de Janeiro (Brazil). *Revista de Gestão Costeira Integrada,* 15(3), 353-370.

PIMENTEL, M. 1762. *Arte de navegar em que se ensinam as regras práticas, e os modos de cartear, e de graduar a balestilha por via de números e muitos problemas uteis à navegação, e roteiro das viagens, e costas marítimas de Guiné, Angola, Brazil, Indias, e Ilhas Occidentais, e Orientaes.* Lisbon: Forgotten Books.

PINHEIRO, T. C., MILEZE, A. M. B. & RIBEIRO, G. P. 2008. *Mapeamento digital no sistema SPRING a partir de dados GPS e imagens sensoriais IKONOS da zona costeira meridional do município de São João da Barra-RJ, como requisito para o planejamento territorial. In:* II Simpósio Brasileiro de Ciências Geodésicas e Tecnologias da Geoinformação (CGTG). Recife, PE, September 8-11, 2008, CGTG, Recife, pp. 1-7.

RIBEIRO, G. P. 2005. *Tecnologias digitais de geoprocessamento no suporte à análise espaço-temporal em ambiente costeiro.* PhD. Niterói: Programa de Pós-Graduação em Geografia da Universidade Federal Fluminense.

RIBEIRO, G. P., ROCHA, C. H. O., FIGUEIREDO JUNIOR, A. G., SILVA, C. G., SILVA, S. H. F., MOREIRA, P. S. C., GUIMARÃES, M. S. D., PEREIRA, A. P., ALMEIDA, A. G., PINNA, B. G., SOUZA, C. F., SILVA, C., SANTOS, R. A. & VASCONCELOS, S. C. 2004. Análise espaço-temporal no suporte à avaliação do processo de erosão costeira em Atafona, São João da Barra (RJ). *Revista Brasileira de Cartografia,* 56(2), 129-138.

RINK W. J. & LÓPEZ, G. I. 2010. OSL-based lateral progradation and aeolian sediment accumulation rates for the Apalachicola Barrier Island Complex, North Gulf of Mexico, Florida. *Geomorphology,* 123(3-4), 330-342.

ROY, P. S., COWELL, P. J., FERLAND, M. A. & THOM, B. G. 1994. Wave-dominated coasts. *In:* CARTER, R. W. G. & WOODROFFE, C. D. (eds.). *Coastal evolution: late quaternary shoreline morphodynamics.* Cambridge: Cambridge University press, pp. 121-186.

RUSS, E. & PALINKAS, C. 2020. Evolving sediment dynamics due to anthropogenic processes in upper Chesapeake Bay. *Estuarine, Coastal and Shelf Science,* 325, e106596.

SALTER, S. H. 1974. Wave power. *Nature,* 249(5459), 720-724.

SANTOS, F. M. & DO CARMO, R. L. 2017. As dimensões humanas das mudanças ambientais: percepção ambiental e estratégias de adaptação em Ilha Comprida–São Paulo. *Journal of Integrated Coastal Zone Management,* 17(2), 117-137.

SAWAKUCHI, A. O., GUEDES, C. C. F., DEWITT, R., GIANNINI, P. C. F., BLAIR, M. W., NASCIMENTO JUNIOR, D. R. & FALEIROS, F. M. 2012. Quartz OSL sensitivity as a proxy for storm activity on the southern Brazilian coast during the Late Holocene. *Quaternary Geochronology,* 13, 92-102.

SAWAKUCHI, A. O., KALCHGRUBER, R., GIANNINI, P. C. F., NASCIMENTO JUNIOR, D. R., GUEDES, C. C. F. & UMISEDO, N. K. 2008. The development of blowouts and foredunes in the Ilha Comprida barrier (Southeastern Brazil): the influence of Late Holocene climate changes on coastal sedimentation. *Quaternary Science Reviews,* 27(21-22), 2076-2090.

SCHAEFFER-NOVELLI, Y., MESQUITA, H. S. L. & CINTRÓN-MOLERO, G. 1990. The Cananéia Lagoon estuarine system, São Paulo, Brazil. *Estuaries,* 13, 193-203, DOI: https://doi.org/10.2307/1351589

SCHNEIDER, U., BECKER, A., FINGER, P., MEYER-CHRISTOFFER, A. & RUDOLF, B. Z. M. 2015. GPCC full data reanalysis version 7.0 at 0.5°: monthly land-surface precipitation from rain-gauges built on GTS-based and historic data. Berlin: Ministry of Health, DOI: https://doi.org/10.5676/DWD_GPCC/FD_M_V7_050

SILVA, G. A. M. & AMBRIZZI, T. 2006. Inter-El Niño variability and its impact on the South American low-level jet east of the Andes during austral summer – two case studies. *Advances in Geosciences,* 6, 283-287.

SILVA, G. A. M. & AMBRIZZI, T. 2010. Summertime moisture transport over Southeastern South America and extratropical cyclones behavior during inter-El Niño events. *Theoretical and Applied Climatology,* 101(3-4), 303-310.

SILVA, G. A. M., AMBRIZZI, T. & MARENGO, J. A. 2009. Observational evidences on the modulation of the South American Low Level Jet east of the Andes according the ENSO variability. *Annales Geophysicae,* 27(2), 645-657.

SILVA, F. G., SOUSA, P. H. G. O. & SIEGLE, E. 2016. Longshore transport gradients and erosion processes along the Ilha Comprida (Brazil) beach system. *Ocean Dynamics,* 66(6-7), 853-863.

SIMÃO JUNIOR., J., CARNESECA, L. F., BARROS, M. T. L., ELIAS JUNIOR., M. J., IKEDA, N. A., SILVA, P. R. N., SILVA, A. P., GUSSO, F. E. N., LANGE, R., MORAES, A. M., LIAZI, A., SILVA, A. P., RAMOS, C. L., MATSUBARA, C. T., TRAMONTI, D. G., NASHIRO, G., MAKIBARA, H., BARROS, J. M. T., MANFREDINI, P., BERTAGNOLI, R. R. & ONO, S. 1998. *Bacia Hidrográfica do Ribeira do Iguape - Plano de Ação Para o Controle das Inundações e Diretrizes Para o Desenvolvimento do Vale.* São Paulo: DAEE (Departamento de Águas e Energia Elétrica do Estado de São Paulo).

SOUZA, T. A. & OLIVEIRA, R. C. 2016. Alterações ambientais no complexo estuarino-lagunar de Cananeia-Iguape: a influência do canal artificial do "Valo Grande". *Boletim de Geografia,* 34(3), 30-44.

SOUZA, C. R. G. & SUGUIO, K. 1996. Coastal erosion and beach morphodynamics along the State of São Paulo (SE Brazil). *Anais Academia Brasileira de Ciências,* 68(3), 405-424.

SUGUIO, K. & MARTIN, L. 1994. Geologia do quaternário. *In:* FALCONI, F. F. & NIGRO JUNIOR, A. (eds.). *Solos do litoral de São Paulo.* São Paulo: Mesa Redonda ABMS/ASSECOB, pp. 69-97.

SUGUIO, K., TATUMI, S. H. & KOWATA, E. A. 1999. The Comprida Island inactive dune ridges and their possible significance for the island evolution during the Holocene, State of São Paulo, Brazil. *Anais da Academia Brasileira de Ciências,* 71(4), 623-630.

SUGUIO, K., TATUMI, S. H., KOWATA, E. A., MUNITA, C. S. & PAIVA, R. P. 2003. Upper Pleistocene deposits of the Comprida Island (São Paulo State) dated by thermoluminescence method. *Anais da Academia Brasileira de Ciências,* 75(1), 91-96.

TAMURA, T. 2012. Beach ridges and prograded beach deposits as palaeoenvironment records. *Earth-Science Reviews,* 114(3-4), 279-297.

TANNER, W. F. 1995. Origin of beach ridges and swales. *Marine Geology,* 129, 149-161.

TESSLER, M. G. 1988. *Dinâmica sedimentar quaternária no litoral sul paulista, Estado de São Paulo.* PhD. São Paulo: Instituto de Geociências da Universidade de São Paulo.

VILES, H. A. & GOUDIE, A. S. 2003. Interannual, decadal and multidecadal scale climatic variability and geomorphology. *Earth-Science Reviews,* 61(1-2), 105-131.

VERA, C., HIGGINS, W., AMBRIZZI, T., AMADOR, J., GARREAUD, R., GOCHIS, D., GUTZLER, D., LETTENMAIER, D., MARENGO, J., MECHOSO, C. R., NOGUES-PAEGLE, J., SILVA DIAS, P. L. & ZHANG, C. 2006. Toward a unified view of the American Monsoon Systems. *Journal of Climate,* 19(20), 4977-5000.

YOUNG, E. G. 1903. História de Iguape. *Revista do Instituto Histórico e Geográfico de São Paulo* [online], VIII, 222-375. Available at: https://archive.org/details/revistadoinstit39unkngoog [Accessed: 15 Aug. 2018].

WINTLE, A. G. & MURRAY, A. S. 2006. A review of quartz optically stimulated luminescence characteristics and their relevance in single-aliquot regeneration dating protocols. *Radiation Measurements,* 41(4), 369-391.

WOODROFFE, C. D. 2002. *Coasts: form, process and evolution*. Cambridge: Cambridge University Press.

ZHANG, R., CHEN, L., LIU, S., ZHANG, H., GONG, W. & LIN, G. 2019. Shoreline evolution in an embayed beach adjacent to tidal inlet: the impact of anthropogenic activities. *Geomorphology,* 346, e106856.

ZHANG, W. Y., HARFF, J., SCHNEIDER, R., MEYER, M., ZORITA, E. & HÜNICKE, B. 2014. Holocene morphogenesis at the southern Baltic Sea: simulation of multi-scale processes and their interactions for the Darss-Zingst peninsula. *Journal of Marine Systems*, 129, 4-18, DOI: https://doi.org/10.1016/j.jmarsys.2013.06.003

ZHOU, J. & LAU, K. M. 1998. Does a monsson climate exist over South America? *Journal of Climate,* 11(5), 1020-1040.